Universidade de Aveiro Departamento de Física,
2017

Jorge Diogo
Marques Laranjeira

Procura de Possíveis Estruturas Cristalinas do Polímero de C_{60} a 9.5GPa pelo Método DFT

Search for Possible Crystal Structures of the 9.5GPa C_{60} Polymer via DFT Methods

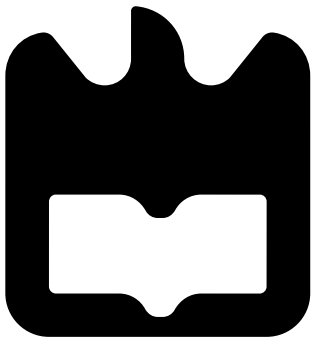

Jorge Diogo
Marques Laranjeira

Procura de Possíveis Estruturas Cristalinas do Polímero de C_{60} a 9.5GPa pelo Método DFT

Search for Possible Crystal Structures of the 9.5GPa C_{60} Polymer via DFT Methods

Jorge Diogo
Marques Laranjeira

Procura de Possíveis Estruturas Cristalinas do Polímero de C_{60} a 9.5GPa pelo Método DFT

Search for Possible Crystal Structures of the 9.5GPa C_{60} Polymer via DFT Methods

Dissertação apresentada à Universidade de Aveiro para cumprimento dos requesitos necessários à obtenção do grau de Mestre em Física, realizada sob a orientação científica de Dr. Leonel Marques Vitorino Joaquim, Professor do Departamento Física da Universidade de Aveiro

the jury

president

Dr. Manuel António dos Santos Barroso
Assistant Professor at Aveiro University

examiners committee

Dr. Leonel Marques Vitorino Joaquim
Assistant Professor at Aveiro University (Advisor)

Dr. José António de Carvalho Paixão
Full Professor at Coimbra University

Acknowledgemens

First of all I would like to show my gratitude to professor Leonel Marques for accepting my request to be my advisor, without his effort and availability this thesis would not be possible. I also appreciate his patience and will to teach me.

I would like to offer my sincere gratitude to professor José António de Carvalho Paixão for accepting to discuss this thesis.

To Manuel Melle-Franco and his student Karol Strutyński for their availability to help me with Density Functional Theory calculations and for all the discussions about this matter.

To Nuno Fortunato for his friendship, availability to discuss Density Functional Theory issues and other matters.

My colleagues Daniel Duarte, João Duarte and José Vieira for their friendship and help with some computer and writing issues.

To Yuriy Skorokhod for accepting me as his Erasmus+ student. I would like to say thanks to the other members of the high pressure laboratory of the Czech Academy of Sciences for all their availability.

To Alexander Tselev for giving me the opportunity to work in Atomic force microscopy with C_{60} samples and all the good discussions about this and other issues that we had.

My brother, Hugo Laranjeira, for his advices in countless issues his friendship and trust.

My father, Artur Laranjeira, for his high standards. My mother, Maria Teresa Claro, for all her help and support.

To finish I would like to show my gratitude to professor Manuel Barroso for all his help and guidance.

Resumo

A Teoria do Funcional da Densidade é usada para investigar possíveis estruturas de uma fase polimérica cúbica de faces centradas de C_{60} obtida a 9.5GPa e 823K.

Verificámos que quando duas orientações moleculares padrão, compatíveis com uma estrutura cúbica, são consideradas, ligações poliméricas do tipo (2+2) cicloadição 5:6(PP) são formadas entre moléculas vizinhas com orientação diferente mas não entre moléculas vizinhas com a mesma orientação. Temos, assim, uma interação análoga à interação antiferromagnética.

Foram estudadas estruturas ordenadas, construídas com as moléculas nestas orientações padrão, no entanto as estruturas obtidas não são compatíveis com o padrão de difração experimental, ou porque as estruturas não apresentam métrica cúbica ou porque a estrutura cúbica obtida dá origem a super-reflexões não observadas experimentalmente.

Estes resultados permitiram-nos concluir, por analogia ao modelo de Ising antiferromagnético com interações entre vizinhos próximos numa rede cúbica de faces centradas, que a estrutura desta fase polimérica de C_{60} deverá ser frustrada em que uma dada molécula está ligada a oito das doze moléculas vizinhas mais próximas.

Abstract

Density Functional Theory methods are used to investigate the possible structure of the face-centered cubic polymeric C_{60} phase obtained at 9.5GPa and 823K.

We have found that when only the standard molecular orientation that are compatible with the cubic structure are considered, polymeric bonds of the (2+2) cycloaddition 5:6(PP) type are formed between nearest neighbor molecules differently oriented but not between nearest neighbor molecules with the same orientation. This is analogous to the antiferromagnetic interaction.

We have studied ordered structures built with molecules in standard orientations, but the obtained structures cannot explain the experimental diffraction pattern, because these structures have not a cubic metric or because they display reflections not observed experimentally.

These results allowed us to conclude, considering that our system can be mapped to the antiferromagnetic Ising model with nearest neighbor interactions in a face centered cubic lattice, that the polymer should have a frustrated structure in which each molecule is bonded to eight out of twelve nearest neighbors.

Contents

List of Figures

List of Tables

Chapter 1

Introduction

In 1985, the discovery of a new carbon allotrope was reported by H. W. Kroto et al. [1], the C_{60} fullerene. Later, in 1990, Krätschmer et al. [2] were able to synthesize it in macroscopic amounts. Since then, physical and chemical properties of C_{60} have been the focus of extensive studies.

At room temperature, C_{60} displays a face centered cubic (fcc) lattice, space group $Fm\bar{3}m$, with a lattice parameter (a_C) of 14.17Å [3] and a distance between the centers of neighboring molecules of 10Å. Van der Waals interactions are responsible to hold such a structure. The molecules have disordered orientations. At 249K solid C_{60} undergoes a first order phase transition to a simple cubic (sc) lattice, space group $Pa\bar{3}$, with a lattice parameter of 14.04Å [4], where C_{60} molecules are orientationally ordered.

In 1993, photoinduced polymerization of C_{60} was reported by A. M. Rao et al. [5] and since then interest in polymerized fullerenes grow. In 1994, pressure induced polymerization of C_{60} was first reported by Iwasa et al. [6].

The application of pressure, besides decreasing intermolecular distance, freezes the molecular rotational motion locking the molecular orientation, on the other hand increasing the temperature leads to rotational disorder. Thus, applying pressure and temperature allows the C_{60} molecules to adopt an optimal orientation allowing the formation of C_{60} polymeric phases.

Up to now, there are four polymeric structures prepared at high pressure and temperature: one dimensional (1D) orthorhombic phase [7, 8], two dimensional (2D) tetragonal and rhombohedral phases [8–10], and a three dimensional (3D) phase called cuboidal C_{60} [11]. This cuboidal phase is not obtained from compressing pristine C_{60} but from compressing the 2D tetragonal phase. A scheme of the C_{60} pressure-temperature diagram is shown in figure 1.1.

Besides experimental studies, fullerene polymerized structures have also been studied with computational methods. The 2D polymerized structures were studied using a local density approximation (LDA) functional within Density Functional Theory (DFT) [12, 13]. We have also performed DFT calculations, using a generalized-gradient approximation (GGA) functional, on the known polymeric structures that will be present later. C_{60} polymerized structures were also studied using other computational methods, like tight-biding [14], molecular dynamics [15] and Hartree-Fock theory [16]. The latter was used to determine C_{60} dimerization energy and covalent bond lengths [16].

Although fullerene phases have been the scope of numerous studies, the 3D polymeric structures are still an enigma to be solved, excepting the cuboidal phase. The present work tries to shed light on structures of 3D polymerized phases.

The low resolution diffraction data characteristic of 3D polymerized phases makes it impossible to solve their crystal structures through x-ray crystallography techniques. Computational methods are thus a viable way to help to find the correct crystal structure. In this thesis,

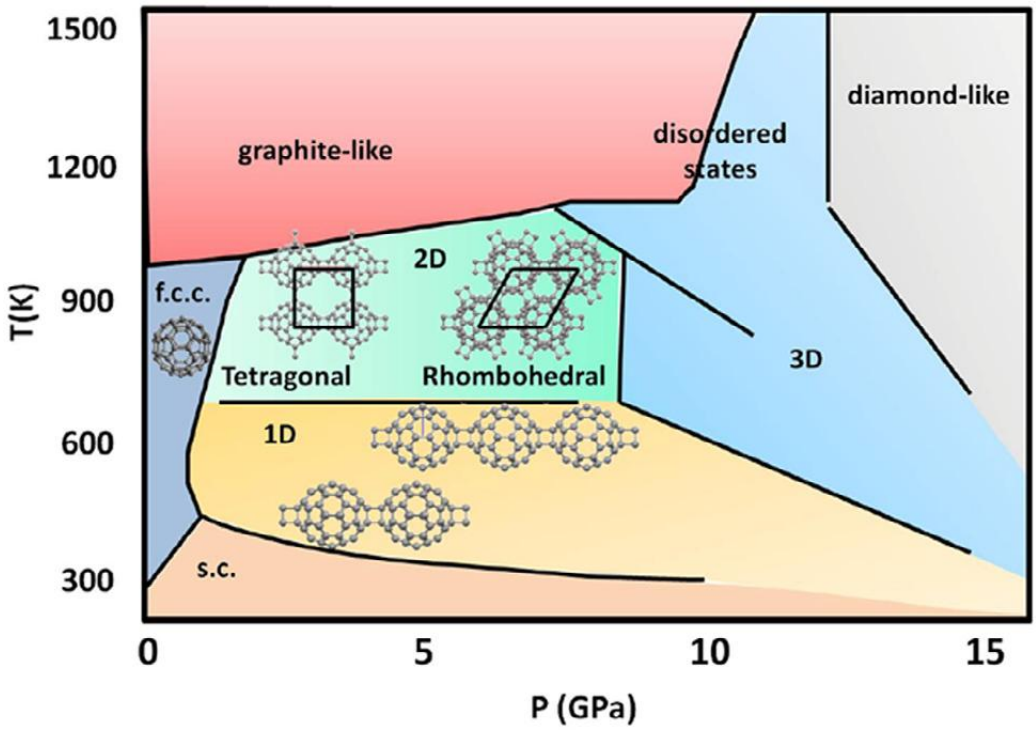

Figure 1.1: Pressure-temperature diagram of C_{60}. Figure from [3].

---

using information from the diffraction pattern (overall symmetry and lattice parameters) we have constructed some idealized structural models which could describe the structure of our 3D polymeric phase. We relaxed such structures with DFT to check their stability and to optimize their structures. We have employed VASP software version 5.4.1 [17–20], which was run in ARGUS, one of the University of Aveiro clusters.

Initially we have tried to use an evolutionary algorithm (USPEX[21–25]) with no success due to the molecular characteristics of our structure.

The thesis is organized as follows:

- Chapter 2 gives some hints of crystallography and diffraction. In the end of this chapter we show the experimental diffraction patterns of the 9.5GPa C_{60} polymer.
- In chapter 3 an explanation of the Density Functional Theory is given.
- In chapter 4 we present some symmetry consideration on the C_{60} molecule and structure, as well as the description of how C_{60} dimers can form. Then we present the state of the art on polymeric C_{60} structures synthesized at pressures lower than 8GPa, and the cuboidal phase.
- In chapter 5 we present the application of DFT methods to 3D C_{60} polymeric structures.
- Finally in chapter 6 we discuss what should be the crystal structure of the polymeric C_{60} phase obtained at 9.5GPa and finish with some concluding remarks.

Most of the images presented in this thesis were made with VESTA [26].

Chapter 2

Crystalline Structure and Diffraction

A crystal lattice may be built from infinite repetitions of a unit cell spanned over three non coplanar vectors $\vec{a_1}$, $\vec{a_2}$ and $\vec{a_3}$, known as lattice vectors. We can understand the previous as a lattice position, $\vec{r'}$, being equivalent to another lattice position, $\vec{r}$, by the following translation vector:

$$\vec{r'} = \vec{r} + n_1\vec{a_1} + n_2\vec{a_2} + n_3\vec{a_3} \tag{2.1}$$

being n_1, n_2 and n_3 any integer number.

A crystal unit cell may be defined as a primitive cell if it has the lowest possible volume for that crystal structure. A centered cell (body centered, face centered, side centered) is not a primitive cell since it may be described in a smaller unit cell.

2.1 Crystal Systems

Crystals are grouped into seven crystal systems that are defined accordingly different unit cell metric specifications. Each space group may be ascribed to one of these systems.

A crystal lattice unit cell has six degrees of freedom. Three lattice parameter $a = a_1$, $b = a_2$, $c = a_3$ and three angles α (defined between a_2 and a_3), β (defined between a_1 and a_3), γ (defined between a_1 and a_2).

The seven crystal systems are distinguished by the specifications given in table 2.1.

Table 2.1: Crystal lattice systems unit cell specifications.

Crystal lattice family	fixed parameters
triclinic	none
monoclinic	$\beta = 90°$
orthorhombic	$\alpha = \beta = \gamma = 90°$
rhombohedral	$a = b = c, \alpha = \beta = \gamma \neq 90°$
hexagonal	$a = b, \alpha = \beta = 90°, \gamma = 120°$
tetragonal	$a = b, \alpha = \beta = \gamma = 90°$
cubic	$a = b = c, \alpha = \beta = \gamma = 90°$

2.2 Miller Indices

Miller indices (hkl) are used to identify the lattice planes. In order to obtain them, we find in the first place the intersection point, (x, y, z) in terms of lattice constants a_1, a_2, a_3.

Obtaining $(\frac{x}{a_1}, \frac{y}{a_2}, \frac{z}{a_3})$. Then we take the reciprocals of these numbers $(\frac{a_1}{x}, \frac{a_2}{y}, \frac{a_3}{z})$ and multiply all of them by the minimum integer value, n, to transform all of them into integers. In this way we get the Miller indices $(n\frac{a_1}{x}, n\frac{a_2}{y}, n\frac{a_3}{z})$.

2.3 Space Groups

Equation (2.1) shows that a crystal is invariant under a certain translation which means that the crystal lattice has translational symmetry elements. Besides such pure translation symmetry it also has other point symmetry elements like mirror plane reflection, inversions and rotations. A crystal structure just allows 1,2,3,4 and 6-fold rotation (degree of each rotation is given in radians by $\frac{2\pi}{n}$ with n being 1,2,3,4,6).

Other elements of symmetry can be obtained from combining translation and point symmetry elements. There exists glide planes as symmetry operations constructed of an mirror plane reflection followed by a translation. Even another symmetry operation is a screw axis that is a rotation followed by a translation.

Table 2.2: Translation symmetry symbols.

translation symmetry	symbol
face-centered	F
body-centered	I
side-centered	A, B, C
rhombohedral	R
primitive	P

Table 2.3: Symmetry elements symbols.

symmetry elements	symbol
mirror plane	m
rotation	1,2,3,4,6
rotation and inversion	$\bar{1}, \bar{2}, \bar{3}, \bar{4}, \bar{6}$
glide planes	*a,b,c,n,d*
screw axes	$2_1, 3_1, 3_2, 4_1, 4_2, 4_3$ $6_1, 6_2, 6_3, 6_4, 6_5$

All these symmetry operations only allow the existence of 230 unique combinations of themselves in a crystal lattice. We call each of these 230 combinations space groups. Table 2.2 shows the symbols for space group symmetry operations.

When writing the space groups symbols of a given structure we first write the translation symmetry accordingly to the table 2.2 followed by the other independent symmetry elements listed in table 2.3.

2.4 Close Packed Structures

Close packed structures were initially introduce to describe the structures of metals and alloys, considering the packing of atoms as packing of spheres. In the close packed structures a packed layer of spheres is placed on top of another with the smallest possible distance as seen in figure 2.1.

The layers can be stacked in two close packed ways. Taking a given layer of such close packed spheres, layer A, there is only one way to put the next layer above it, layer B. For the third layer we have two options: we may put this layer as the first one A, as seen in 2.1(a), or in a new position, layer C, as seen in figure 2.1(b). These stackings lead to two distinct structures one where the AB stacked layer combination is repeated and another one where the ABC is the repeated unit.

The face centered cubic structure is a closed packed structure of ABC stacking while AB stacking is an hexagonal closed packed structure. Both have a volume occupation ratio of 74%.

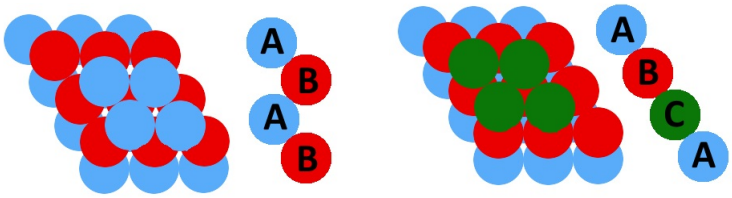

(a) (b)

Figure 2.1: Stacking of packed layers. (a) ABAB... stacking. (b) ABCABC... stacking.

2.5 Crystal Diffraction

When a crystalline structure is irradiated by a beam having a wavelength with magnitude of the same order of the lattice parameters, a diffraction pattern will be produced. This diffraction pattern gives information about the lattice of such structure in the reciprocal space, the Fourier space. X-ray photons, electrons and neutrons have the appropriate wavelength to obtain a crystal diffraction pattern.

2.5.1 Bragg's Law

In 1913, H. Bragg and W. Bragg enunciated a constructive interference condition that allows to relate the distance between lattice planes, d, of the same family (hkl) and the incident beam wavelength, λ:

$$2d \sin\theta = n\lambda \tag{2.2}$$

θ being the angle made by the incident beam in the lattice planes and n an integer. This condition is named Bragg's law.

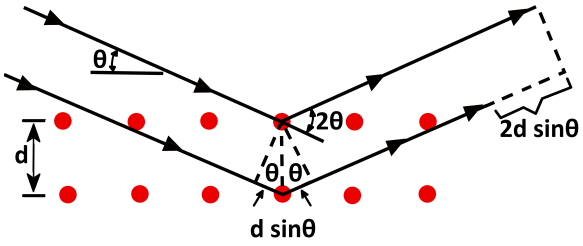

Figure 2.2: Bragg diffraction from two parallel atom layers.

Figure 2.2 illustrates the process. Two waves scattered by two lattice planes will interfere constructively if the path difference is a multiple integer of the wavelength, $n\lambda$, otherwise they will cancel, when a large number of lattice planes is considered. The path difference between two waves in two distinct planes is $2d \sin\theta$ and thus we arrive at Bragg equation of constructive interference $2d \sin\theta = n\lambda$.

2.5.2 Systematic Extinctions

In x-ray diffraction by certain crystal structures there is some lattice planes whose intensity reflections are absent. Such reflections are not allowed because of the crystal symmetry, in particular translational symmetry operations, glide planes and screw axes. The identification of

these systematic extinctions provides useful information for the determination of the crystalline structure.

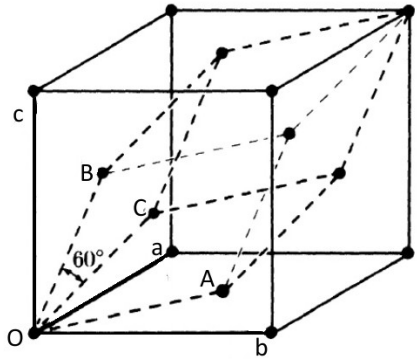

Figure 2.3: Rhombohedral cell ascribed into an fcc lattice.

Lets obtain these systematic extinctions for an fcc lattice with $\vec{a}$, $\vec{b}$ and $\vec{c}$ lattice vectors. Consider the primitive unit cell of such structure (rhombohedral cell) with $\vec{A}$, $\vec{B}$ and $\vec{C}$ lattice vectors, (see figure 2.3) one can write the transformation equations of one cell into another:

$$\begin{array}{l} \vec{A} = \frac{1}{2}\vec{a} + \frac{1}{2}\vec{b} + 0\vec{c} \\ \vec{B} = \frac{1}{2}\vec{a} + 0\vec{b} + \frac{1}{2}\vec{c} \\ \vec{C} = 0\vec{a} + \frac{1}{2}\vec{b} + \frac{1}{2}\vec{c} \end{array} \tag{2.3}$$

The Miller indices transform in the same way as the lattice vectors:

$$\begin{array}{l} \vec{H} = \frac{1}{2}\vec{h} + \frac{1}{2}\vec{k} + 0\vec{l} \\ \vec{K} = \frac{1}{2}\vec{h} + 0\vec{k} + \frac{1}{2}\vec{l} \\ \vec{L} = 0\vec{h} + \frac{1}{2}\vec{k} + \frac{1}{2}\vec{l} \end{array} \tag{2.4}$$

(HKL) being the Miller indices of the rhombohedral cell and (hkl) the Miller indices of the fcc cell.

The Miller indices have to be integers, thus:

$$2H = h + k, \quad 2K = h + l, \quad 2L = k + l \tag{2.5}$$

As the indices H, K, L are integers $(h + k)$, $(h + l)$ and $(k + l)$ are all even. An even number is the sum of two even number or two odd numbers. So we conclude that the planes that will present reflections, in an fcc lattice, have all even or all odd Miller indices: (111), (200), (220), (311), (222), ...

2.6 Experimental Diffraction Pattern

Our C_{60} polymerized sample was prepared by applying pressure up to 9.5GPa and then temperatures of 823K in a Paris–Edinburgh press [27]. X-ray diffraction patterns were obtained in situ at the European Synchrotron Radiation Facility (ESRF) Grenoble, France by Professor Dr. Leonel Marques at different pressure conditions, and are shown in figure 2.4, together with the diffraction pattern of the background originated by the sample assembly and the diffraction pattern of starting C_{60}. The beam wavelength was 0.53396Å.

As referred above, an fcc lattice displays reflections which have Miller indices all odd or all even. Accordingly, the indexation of the reflections is given in figure 2.4.

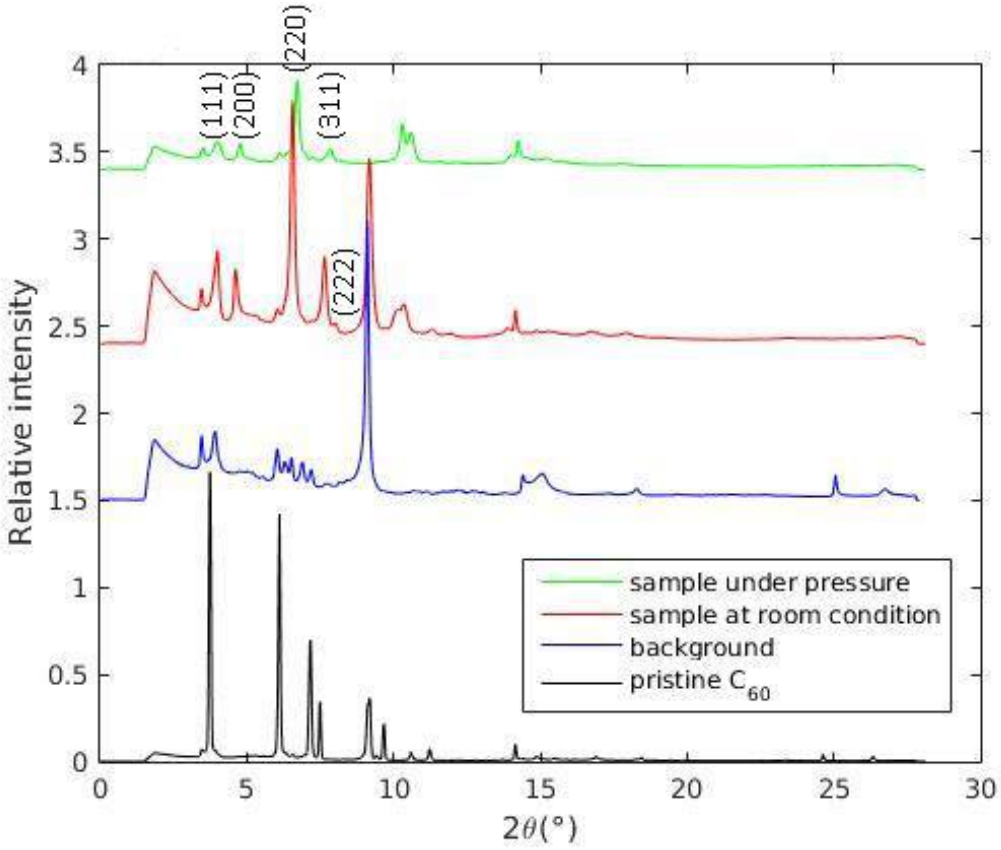

Figure 2.4: Sample, background and pristine C_{60} diffraction patterns and sample peak Miller indices.

From geometric considerations the interplane distance of the (hkl) lattice planes of a cubic lattice is given by:

$$d_{(hkl)} = \frac{a_c}{\sqrt{h^2 + k^2 + l^2}} \tag{2.6}$$

where a_c is the cubic lattice parameter. Considering the first order diffraction, $n = 1$, from joining equations (2.2) and (2.6) one can write:

$$a_c = \frac{\lambda\sqrt{h^2 + k^2 + l^2}}{2\sin(\theta)} \tag{2.7}$$

Applying this equation to the above x-ray diffraction patterns a lattice parameter of 13.19 ± 0.02Å was obtained at room conditions and 12.74 ± 0.02Å at high pressure. The corresponding nearest neighbor distance is 9.33Å at room conditions and 9.01Å under pressure. Note that Bragg peaks from the C_{60} diffraction patterns are observed only up to $2\theta \approx 20°$, indicating that the lattice is ordered to a certain degree.

Chapter 3

Density Functional Theory

The following DFT description is mostly based on reference [28].

Through the Schrödinger equation one can describe quantum physics problems if one has the system's wave function. The single electron Schrödinger equation is written as:

$$\left[-\frac{\hbar^2\nabla^2}{2m} + v(\vec{r})\right]\psi(\vec{r}) = E\psi(\vec{r}) \tag{3.1}$$

here $\psi(\vec{r})$ is the electron wave function, $v(\vec{r})$ is a potential acting on the electron (for instance nuclear potential), $\vec{r}$ is the position vector, m is the electron mass, $\hbar$ is the Planck constant over 2π and ∇^2 is the laplacian.

Considering more than one electron Schrödinger equation takes the form:

$$\left[\sum_i^N \left(-\frac{\hbar^2\nabla_i^2}{2m} + v(\vec{r_i})\right) + \sum_{i<j} U(\vec{r_i}, \vec{r_j})\right]\psi(\vec{r_1}, \vec{r_2}, ..., \vec{r_N}) = E\psi(\vec{r_1}, \vec{r_2}, ..., \vec{r_N}) \tag{3.2}$$

N is the number of electrons and $U(\vec{r_i}, \vec{r_j})$ is the Coulomb interaction between electrons, with charge q, defined as follows:

$$\hat{U} = \sum_{i<j} U(\vec{r_i}, \vec{r_j}) = \sum_{i<j} \frac{q^2}{|\vec{r_i} - \vec{r_j}|} \tag{3.3}$$

We can also take the kinetic operator as:

$$\hat{T} = -\frac{\hbar^2}{2m}\sum_i \nabla_i^2 \tag{3.4}$$

As $\hat{T}$ and $\hat{U}$ are system invariant the nature of our system just depends on $v(\vec{r_i})$. For a many body system the $v(\vec{r_i})$ potential can be written as:

$$\hat{V} = \sum_i v(\vec{r_i}) = \sum_{ik} \frac{Q_k q}{|\vec{r_i} - \vec{R_k}|} \tag{3.5}$$

k denotes every nuclei in the system with charge Q_k and position $\vec{R_k}$. Within this potential just the nuclei position and boundary conditions differentiate a molecule from a solid. In the same way what differentiates the single body problem and the many body problem is the term due to Coulomb interaction.

To solve Schrödinger's equation usually we specify the system's potential, then we solve the equation to find the corresponding wave function, from these we can calculate the observables.

This may seem easy, however, when it is a many body problem this equation is impossible to solve in both analytical and numerical ways.

Density functional theory (DFT) allows us to approximately solve the many body Schrödinger equation enabling the calculation of, for instance, the phonon spectra, the bulk moduli, and the structure energy in crystalline structures.

Within DFT all electronic systems differ only in their potential, $v(\vec{r})$. A way to deal with kinetic and coulomb operators is also given by the technique. DFT also gives a way to map a many body problem into a single body one. This is done using the electronic density, $n(\vec{r})$, as a key variable upon which all other variables can be calculated, reducing a $3N$ variables problem to a N (number of electron in the system) variables one.

The electronic density is given by

$$n(\vec{r}) = N \int d^3\vec{r_2} \int d^3\vec{r_3} ... \int d^3\vec{r_N} \psi * (\vec{r}, \vec{r_2}, ..., \vec{r_N}) \psi(\vec{r}, \vec{r_2}, ..., \vec{r_N}) \tag{3.6}$$

This is possible since knowing the electronic density implies that the system's wave function and potential are known. If we know the wave function and the potential we know all the system variables.

3.1 The Hohenberg-Kohn Theorem

The Hohenberg-Kohn (HK) theorem states that if a ground state electronic density, $n_0(\vec{r})$ is known, it is possible to calculate the ground state wave function, $\psi_0(\vec{r_1}, \vec{r_2}, ..., \vec{r_N})$ that corresponds to that density.

The ground state wave function besides reproducing the ground state electronic density has to minimize the energy:

$$E_v(n_0) = \min_{\psi \to n_0} \left\langle \psi \left| \hat{T} + \hat{U} + \hat{V} \right| \psi \right\rangle \tag{3.7}$$

$E_v(n_0)$ is the ground state energy in a potential of $v(\vec{r})$.

If instead of the ground state density another density (n) is used, then the wave function that produces this density is not the ground state one and the energy minimum found will be larger or equal to the ground state energy minimum.

Since the kinetic and Coulomb operators are system independent we can write the total energy functional as:

$$E_v(n) = \min_{\psi \to n} \left\langle \psi \left| \hat{T} + \hat{U} \right| \psi \right\rangle + \int d^3\vec{r} n(\vec{r}) v(\vec{r}) \tag{3.8}$$

where $\int d^3\vec{r} n(\vec{r}) v(\vec{r}) = V(n)$ is the only system dependent functional. Once the system is known the functional, $V(n)$, is known explicitly.

We can write the energy functional as

$$E(n) = T(n) + U(n) + V(n) \tag{3.9}$$

3.2 DFT as a Single-body Theory

Until now we have discussed DFT as a minimization of an energy functional although this is not the most effective way to implement this theory. Usually one uses the Kohn-Sham approach that does not work with just the electronic density, but also uses single particle wave functions making DFT look like a single particle theory.

We can decompose the kinetic energy functional, $T(n)$, into the kinetic energy of noninteracting particles of electronic density n, $T_s(n)$, and what is left, $T_c(n)$:

$$T(n) = T_s(n) + T_c(n) \tag{3.10}$$

$T_s(n)$ cannot be known, exactly, from the electronic density functional. However, since for noninteracting particles the total kinetic energy is the sum of the individual kinetic energies, it may be written as a sum of single-particle orbitals, $\phi(\vec{r})$, of a noninteracting system:

$$T_s(n) = -\frac{\hbar^2}{2m}\sum_i^N \int d^3\vec{r}\phi_i^*(\vec{r})\nabla^2\phi_i(\vec{r}) \tag{3.11}$$

Since all the orbitals ϕ_i are functionals of the density n we can write that $T_s(n) = T_s(\{\phi_i(n)\})$. Considering the previous equation we can define the exchange-correlation energy functional as:

$$E_{xc}(n) = T_c(n) + U(n) - U_H(n) \tag{3.12}$$

This allow us to rewrite the energy functional as:

$$E(n) = T_s(\{\phi_i(n)\}) + U_H(n) + E_{xc}(n) + V(n) \tag{3.13}$$

As the exchange-correlation energy functional is unknown, the functional is approximated in several ways like local-density approximation (LDA), generalized-gradient approximation (GGA), etc. We will discuss these functionals later.

As the equation (3.13) includes $T_s(n)$, that is now written as a sum of orbitals, one cannot minimize the energy functional with respect to the electronic density n. This was overcome by Kohn and Sham. They started by writing the minimization as:

$$0 = \frac{\delta E[n]}{\delta n(\vec{r})} = \frac{\delta T_s[n]}{\delta n(\vec{r})} + \frac{\delta V[n]}{\delta n(\vec{r})} + \frac{\delta U_H[n]}{\delta n(\vec{r})} + \frac{\delta E_{xc}[n]}{\delta n(\vec{r})} = \frac{\delta T_s[n]}{\delta n(\vec{r})} + v(\vec{r}) + v_H(\vec{r}) + v_{xc}(\vec{r}) \tag{3.14}$$

where we take $\delta V[n]/\delta n(\vec{r}) = v(\vec{r})$, $\delta U_H[n]/\delta n(\vec{r}) = v_H(\vec{r})$ and for $\delta E_{xc}[n]/\delta n(\vec{r})$ we can just calculate it after choosing one of the approximations, for simplicity lets write $\delta E_{xc}[n]/\delta n(\vec{r}) = v_{xc}(\vec{r})$.

Considering a system of noninteracting particles in a potential $v_s(\vec{r})$, where $v_H(\vec{r}) = v_{xc}(\vec{r}) = 0$, the energy minimization will be of the form:

$$0 = \frac{\delta E_s[n]}{\delta n(\vec{r})} = \frac{\delta T_s[n]}{\delta n(\vec{r})} + \frac{\delta V_s[n]}{\delta n(\vec{r})} = \frac{\delta T_s[n]}{\delta n(\vec{r})} + v_s(\vec{r}) \tag{3.15}$$

If we define $v_s(\vec{r})$ to be the following sum:

$$v_s(\vec{r}) = v(\vec{r}) + v_H(\vec{r}) + v_{xc}(\vec{r}) \tag{3.16}$$

Equations (3.14) and (3.15) will have the same solution. By this way it is possible to calculate the electronic density of a many body system by solving a single body system.

The Schrödinger equation of this auxiliary system will be:

$$\left[-\frac{\hbar^2\nabla^2}{2m} + v_s(\vec{r})\right]\phi_i(\vec{r}) = \epsilon_i\phi_i(\vec{r}) \tag{3.17}$$

The $\phi_i(\vec{r})$ orbitals reproduce the electronic density as follows:

$$n_s(\vec{r}) = \sum_i^N f_i|\phi_i(\vec{r})|^2 \tag{3.18}$$

f_i is the occupation of the i'th orbital.

Equations (3.16) and (3.18) are the so called Kohn-Sham (KS) equations.

Solving the KS equations is a nonlinear problem. To solve it, we start with an electronic density guess, $n(\vec{r})$, then calculate the corresponding potential, $v_s(\vec{r})$ and after solve the equation (3.17) and take out the orbitals wave functions, $\phi_i(\vec{r})$. Then the equation (3.18) is used to calculate a new electronic density and the calculation is restarted with this new density (we can also use a mixture of the old and new densities for the new calculations). This process is repeated until convergence (the convergence criteria may be energy, electronic density itself or any system observable), this is a self-consistency cycle.

3.3 DFT Implementation

To implement DFT, normally, one expand the orbitals ϕ_i in a set of suitable basis functions and then solve equation (3.17).

There are different ways to build these basis functions, which are divided in two major groups: the fixed basis functions that are independent of the energy (examples of this are plane-wave expansion and thigh binding) and the ones where the basis functions are energy dependent (for instance augmented plane wave).

Among DFT techniques it is also usual to consider that binding in molecules and solids is mostly due to the valence electrons of the atom. In this way one can consider that the orbitals of the core electrons are almost environment independent so the electronic core and nuclei are seen as an effective "nucleus". Now that the core electrons are accounted in the nuclei description of the atom their calculation will also be included in the atomic calculations leaving just the valence electrons density to calculate in the self-consistency cycle. The nuclei plus electronic core description is called pseudopotential (PP). This method is very useful since it reduces the number of electron treated explicitly by plane wave basis-sets.

Projector augmented-wave method (PAW) is a technique that generalizes PP and linear augmented plane waves, and it was introduced by Böchl [29]. This is the technique that will be used in VASP software.

3.3.1 Reciprocal Space

The solution to Schrödinger's for a periodic system, like a crystal, must satisfy the Bloch theorem which says that the solution can be expressed as follows:

$$\phi_i(\vec{r}) = e^{(i\vec{K}\cdot\vec{r})} u_i(\vec{r}) \tag{3.19}$$

where $\vec{K}$ is the position vector in the reciprocal space and $u_i(\vec{r})$ a periodic function $u_i(\vec{r}) = u(\vec{r} + n_1\vec{a_1} + n_2\vec{a_2} + n_3\vec{a_3})$ with $\vec{a_1}$, $\vec{a_2}$ and $\vec{a_3}$ being crystalline lattice vectors and n_1, n_2 and n_3 integers.

In such way we may try to solve Schrödinger's equation for each K point. This comes handy since many DFT problems are more convenient to solve in the reciprocal space than in the real space. The previous considerations lead us to have to integrate in the reciprocal space which take a lot of computational effort.

In 1976, Monkhorst and Pack [30] developed a solution to this problem. To use their method it is only needed to specify the number of K points required in each direction of the reciprocal lattice.

Increasing the number of K point increase the solution accuracy. As the reciprocal space vectors are inversely proportional to the real space vectors if the lattice parameter increase we may decrease the number of K points and still have an accurate solution.

The number of K points may also be reduced due to symmetry operations within the Brillouin zone[1] (BZ). These symmetries reduce the BZ to the irreducible Brillouin zone (IBZ) which is the part of BZ needed to calculate every integrals. The IBZ may be extended without any approximation to retrieve the BZ. This reduction in the reciprocal space is needed for the calculation and is usually done by the software (VASP includes this reduction).

To ensure a good accuracy one should converge the K points for certain structures.

3.3.2 Energy Cutoff

As $u_i(\vec{r})$ is periodic it can be expanded in a set of plane waves:

$$u_i(\vec{r}) = \sum_j c_j e^{i(\vec{G}\cdot\vec{r})} \tag{3.20}$$

where c_j is a coefficient and $\vec{G} = m_1\vec{b_1} + m_2\vec{b_2} + m_3\vec{b_3}$ being m_1, m_2, m_3 integers and $\vec{b_1}$, $\vec{b_2}$, $\vec{b_3}$ the reciprocal lattice vectors. This vectors are defined as follows:

$$\vec{b_1} = 2\pi\frac{\vec{a_2}\times\vec{a_3}}{\vec{a_1}\cdot(\vec{a_2}\times\vec{a_3})} \quad \vec{b_2} = 2\pi\frac{\vec{a_3}\times\vec{a_1}}{\vec{a_2}\cdot(\vec{a_3}\times\vec{a_1})} \quad \vec{b_3} = 2\pi\frac{\vec{a_1}\times\vec{a_2}}{\vec{a_3}\cdot(\vec{a_1}\times\vec{a_2})} \tag{3.21}$$

with $\vec{a_1}$, $\vec{a_2}$ and $\vec{a_3}$ being the lattice vectors.

From equations (3.19) and (3.20) we can write:

$$\phi_i(\vec{r}) = \sum_j c_{i+j} e^{i(K+G)\vec{r}} \tag{3.22}$$

This equation can be taken as solution of the Schrödinger equation with kinetic energy [31]:

$$T = \frac{h^2}{2m}|\vec{K} + \vec{G}|^2 \tag{3.23}$$

Solution with lower energies have greater importance than solutions with higher values of energy. Because of the above, we truncate the kinetic energy at some value:

$$T_{cut} = \frac{h^2}{2m}G_{cut}^2 \tag{3.24}$$

The previous infinite sum (3.22) takes the following shape:

$$\phi_i(\vec{r}) = \sum_{|j+i|<G_{cut}} c_{i+j} e^{i(K+G)\vec{r}} \tag{3.25}$$

This energy cutoff is important to have good accuracy. Normally, it is easier to define than the K points since most DFT packages have good enough default values.

3.4 Exchange-correlation Functionals

The exchange-correlation potential, $E_{xc}[n]$, are complex, fortunately they yield values much smaller than the known functionals, V, U_H and T_s. This allow us to reasonably approximate this functional.

There are lots of approximations with different features like, for instance local density approximation (LDA) that is a local functional, generalized-gradient approximation (GGA)

[1] The Brilluin zone is a structure primitive cell defined in the reciprocal space.

and gradient-expansion approximations (GEA) which are gradient dependent functionals, Meta-GGA and self-interaction correction (SIC) that are non local functionals, etc.

GGA, in particular PBE (functional proposed in 1996 by Perdew, Burke and Ernzerhof [32, 33]), was used for our VASP software calculations.

The main difference between these two functionals is that in LDA we assume that the density is known at each point, this density varies in space, and its variation rate is accounted for in GGA. In principal GGA describes a problem better than LDA.

Meta-GGA besides taking into consideration the density variation ratio also considers the variation ratio of the density variation ratio. Hyper GGA, is another kind of functional that uses mixtures of exact exchange and GGA exchange functional to describe exchange.

Normally it is introduced the concept of "Jacob's" ladder, shown in figure 3.1, that illustrates the standard categorization of the functional where each rung indicates one step closer to the "perfect" method.

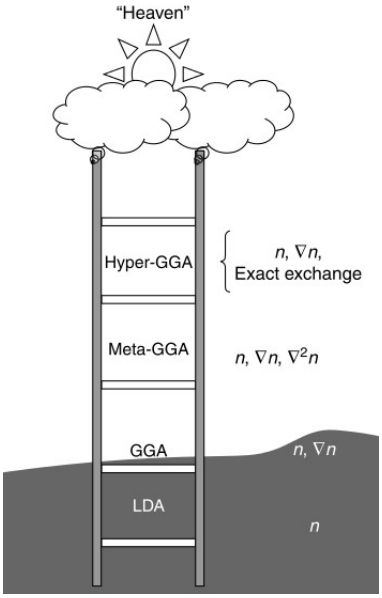

Figure 3.1: "Jacob's" ladder, illustration of Perdew classification of functionals. The physical information used in each functional is written on the right. Figure from [31].

3.4.1 Major Differences Between LDA and GGA Functionals

This subsection was mostly based upon chapters 10.3.3 and 10.3.4 of [31].

Although they are approximations, all these functionals should verify some properties like the sum rule $\int d^3\vec{r'} n_{xc}(\vec{r}, \vec{r'}) = -1$ verified by both. Or the Lieb-Oxford bound:

$$E_{xc}[n] \geq -1.68e^2 \int d^3\vec{r} n(\vec{r})^{4/3} \tag{3.26}$$

that is verified by all LDA and by most GGA functionals. There are more properties that we will not discuss here including ones that both functionals fail to reproduce.

Both this functionals seem to give reliable solutions for almost all chemical bonds although for Van der Waals interactions standard LDA and GGA fail.

Milman et al. [34] optimized several inorganic crystal and molecular compounds structures using a PW91, which is a GGA functional. In majority their calculations yielded bond lenght and lattice parameters errors lower or equal to 2% when comparing with experimental values.

Philipsen and Baerads [35] examined the bulk modulus of eleven solids using the same PW91 functional. Their absolute errors had smaller values than the analogue calculation using an LDA functional. In some specific examples this tendency was not verified.

Considering adsorption and bond energies the trend is kept. GGA gives better results than LDA. In the case of bond energies they are overpredicted. Within GGA PBE shows better solutions than PW91. Hammer et al. [36] presented a revision to PBE functional that shows even better results, this revision was called RPBE.

Funchs et al. [37] took in consideration N_2 bond energy and performed calculations with several functionals concluding that LDA overbinds the molecule in 1eV/atom which is reduced to 0.5eV/atom with PBE and to 0.2eV/atom using RPBE.

Chapter 4

C_{60} Structure

4.1 C_{60} Symmetry

The atoms in the C_{60} molecule are located at the vertexes of a truncated icosahedron, with $m\bar{3}\bar{5}$ molecular point symmetry. A regular icosahedron is a geometric solid with 20 equilateral triangle shaped faces, 30 edges and 12 corners. Figure 4.1 illustrates how to derive a truncated icosahedron from a regular one. What we need to do is to "cut" a plane perpendicular to the vector that connects the icosahedron center to each vertex. In this way, the final geometrical solid will have 12 pentagons and 20 hexagons making a total of 32 faces, 90 edges and 60 corners.

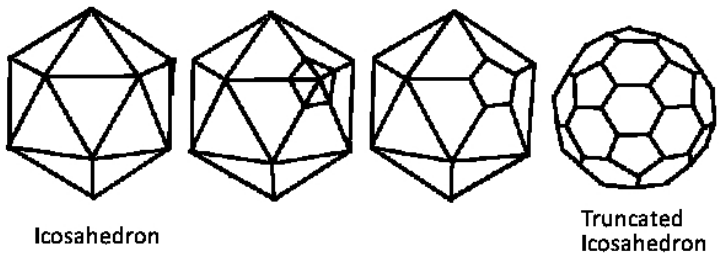

Figure 4.1: From icosahedron to truncated icosahedron.

The hexagons, in the C_{60} molecule, are not regular having two edge lengths. The bonds belonging to hexagons and pentagons are the longer ones (1.45Å) and are single bonds. The ones belonging just to hexagons are shorter double bonds (1.40Å) [38]. The hexagonal faces are, then, perpendicular to 3-fold rotation axes and pentagonal faces are perpendicular to 5-fold rotational axes [4]. The molecule has a center of symmetry and its double bonds are perpendicular to a 2-fold rotation axis, having a mirror plane perpendicular to it.

4.1.1 Standard C_{60} Orientations

In the standard orientations of the C_{60} molecule the intramolecular double bonds, fusing two hexagons, are orthogonal to three cubic axes (see figure 4.2). One standard orientation can be converted into the other through a 90° rotation around any $\langle 100 \rangle$ direction or by a 75.5° rotation around any $\langle 111 \rangle$ direction.

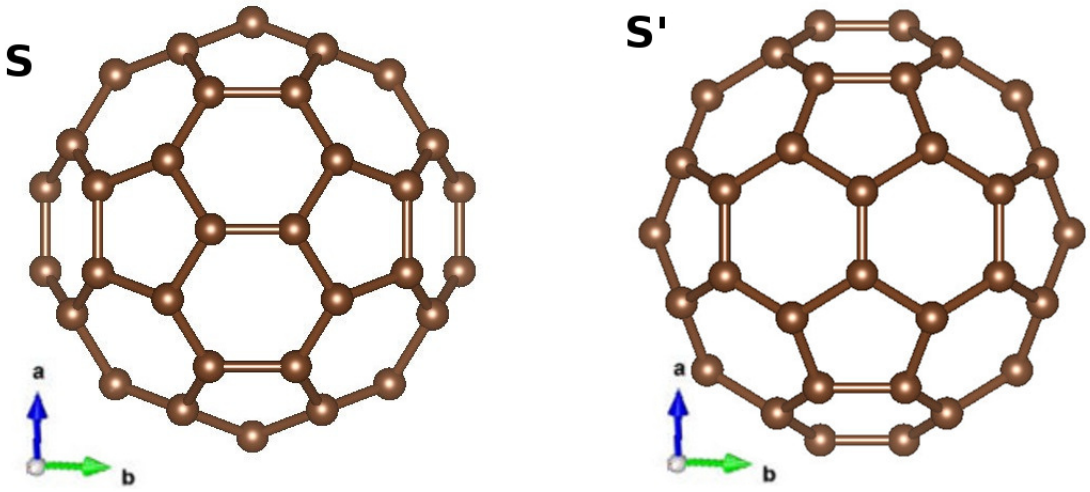

(a) (b)

Figure 4.2: C_{60} molecules standard orientations. (a) C_{60} molecule standard orientation, S. (b) C_{60} molecule standard orientation, S'.

4.1.2 C_{60} Solid Structure at Room Conditions

The C_{60} solid structure at room temperature can be interpreted as an ABC stacking of interacting spheres hold on by Van der Waals interactions. Constructing an fcc lattice with C_{60} molecules in the same standard orientation leads to a $Fm\bar{3}$ space group, the five-fold symmetry being incompatible with crystal symmetry [39].

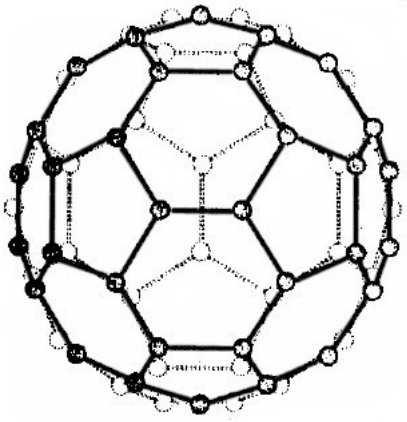

Figure 4.3: C_{60} molecular structure. The dashed lines indicates an example of orientational disorder. Figure from [39].

X-ray diffraction intensities indicate orientational molecular disorder. This disorder can be achieved by the superposition of the two standard orientations, as shown in figure 4.3, leading to a symmetry $Fm\bar{3}m$.

Nuclear magnetic resonance spectroscopy data support a rotating molecule indicating that disorder is higher than the disorder between the two standard orientations, just referred. A model where C_{60} is considered a spherical shell of charge (complete orientational disorder) agree even better with the x-ray diffraction intensities [4].

4.2 C_{60} Dimerization

In 1993, C_{60} dimer was first reported by Rao et al. [5]. They reported the formation of a dimer through (2+2) cycloaddition reactions [6:6] via photoreaction. To achieve the dimer, fcc C_{60} was irradiated with visible or ultra-violet light leading to a new solid structure where molecules are bonded and the fcc structure is kept. Later Davydov et al. [40] produced pressure induced dimerization.

A 6:6 cycloaddition reaction occurs when two new covalent single bonds are formed from a previous two covalent double bonds to create a square ring of atoms. The classification of this reactions is given by the number of atoms that each reacting molecule has in the square ring [41].

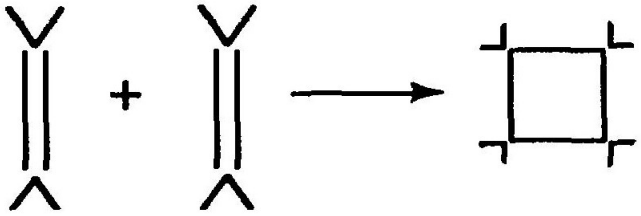

(a)

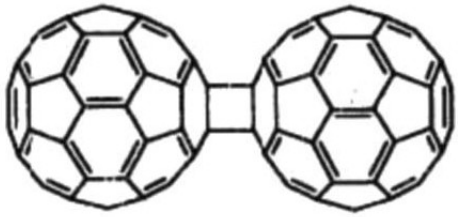

(b)

Figure 4.4: (2+2) cycloaddition reaction. (a) (2+2) cycloaddition reaction. Each angle symbol vertex is an atom and each line is a single bond. Figure from [5]. (b) Two C_{60} molecules bonded via (2+2) cycloadittion reaction 6:6. Figure adapted from [5].

As seen in figure 4.4(a) a (2+2) cycloaddition reaction [6:6] needs two double bonds aligned in order for two C_{60} molecules to bond in this way, as seen in figure 4.4(b). As explained previously, in the C_{60} molecule the double bonds are in the joining of two hexagons, so we call them 6:6 (hexagon-hexagon) bonds.

4.2.1 Other C_{60} Polymer Bonds

C_{60} molecules can be bonded via more chemical schemes than previous (2+2) cycloaddition reaction [6:6]. In theoretical studies Scuseria [16] consider dimerization via (2+2) cycloaddition [6:6], as seen in figure 4.4(b), and via single bond, as seen in figure 4.5(a), concluding that the lowest energy dimer is the one formed via (2+2) cycloadditions [6:6]. In the high pressure polymerized structures obtained below 8GPa, C_{60} molecules are bonded via (2+2) cycloadditions [6:6]. Structural studies preformed by Yamanaka et al.[11] for the 3D cuboidal phase indicated that a (3+3) cycloaddition is involved.

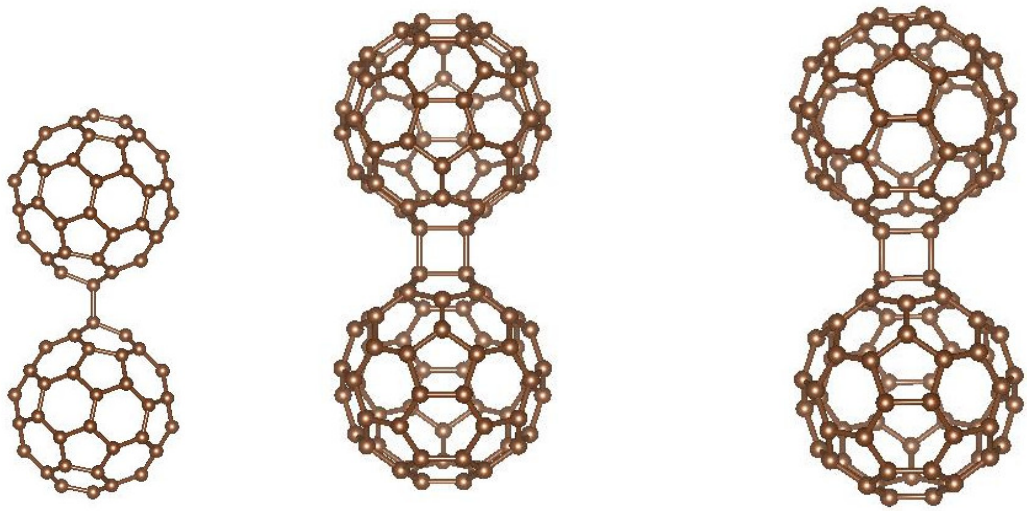

(a) (b) (c)

Figure 4.5: Theoretical dimers. (a) Single bond dimer. (b) (2+2) cycloadittion 5:6(PP-SS) dimer. (c) (2+2) cycloadittion 5:6(PP-OS) dimer.

In the present study we will also consider bonding established between intramolecular hexagon-pentagon bonds (single bonds), this bonding being also a (2+2) cycloaddition. For such bonding, two molecular configuration can be considered. In one case the molecules have different orientation [5:6(PP-SS)], as seen in figure 4.5(b), in the second case the molecules have the same orientation [5:6(PP-OS)], as seen in figure 4.5(c). There is also another possible cycloaddition bonding configuration where a double bond from one molecule is in face of a single bond from another [5:6(HP)], not shown in any figure. Manuel Melle-Franco and Karol Strutyński, from CICECO University of Aveiro, studied these different bonding configurations. They used all-electron calculations performed using Gaussian09 software [42] with a double zeta plus polarization basis set within the LCAO approximation with the PBE functional. The final dimer intermolecular distance yielded is presented in table 4.1. Manuel Melle-Franco and Karol Strutyński kindly provided all the data to us. Manuel Melle-Franco had previously made similar calculations [43].

Table 4.1: Distances between the molecular mass centers for the bonded C_{60} dimers.

Dimer	Intermolecular distance (Å)
single	9.307
6:6	9.112
5:6(HP)	9.133
5:6(PP-OS)	9.156
5:6(PP-SS)	9.161

The dimer with the shorter intermolecular distance is the 6:6 one and then by increasing intermolecular distance we have the 5:6(HP), 5:6(PP-OS), 5:6(PP-SS) and finally the single bond dimer has the largest intermolecular distance.

4.3 C_{60} Polymeric Structures

As referred before, there are four known ways in which the C_{60} molecules form a polymeric structure. The 1D orthorhombic, 2D tetragonal and rhombohedral and the 3D cuboidal. The polymerization process is known to start with the formation of dimers which in turn join together to form higher oligomers and in the end an extended polymer structure is formed.

4.3.1 1D Orthorhombic Phase

The 1D orthorhombic phase is prepared at pressures lower than 2GPa and temperatures between 500K and 700K (see table 4.2). Table 4.2 also summarizes the lattice parameters of this structure. C_{60} molecules are bonded via (2+2) cycloaddition 6:6, as seen in figure 4.6. The C_{60} polymeric chains run along one of the six [110] cubic directions, which means that they form along the shorter a parameter ([100] orthorhombic directions). We can look at this polymer structure as distorting the initial fcc lattice into an orthorhombic lattice (figure 4.6).

Table 4.2: Crystallographic data of 1D orthorhombic phase.

Report on	Phase	space group	a(Å)	b(Å)	c(Å)	P(GPa)	T(K)	Refs.
Powder	O	$Immm$	9.26	9.88	14.22	2.0	573	[8]
Powder	O	$Immm$	9.09	9.83	14.72	1.5	723	[7]
Single Crystal	O	$Pmnn$	9.14	9.90	14.66	1.2	585	[44]
DFT	O	$Immm$	9.11	10.57	15.60	-	-	our calculations

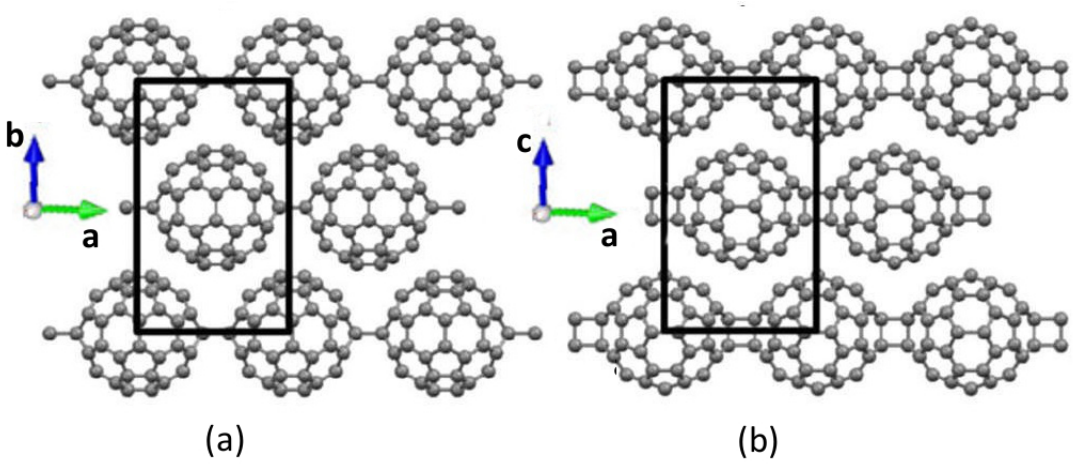

Figure 4.6: Orthorhombic C_{60} phase for different orientations of the chains. (a) Seen perpendicular to the plane defined by a (along the chain formation) and b orthorhombic axes. (b) Seen perpendicular to the plane defined by a (along the chain formation) and c orthorhombic axes. Figure adapted from [3].

We have optimized this structure, the cell parameters and the atomic coordinates. The obtained results are indicated in the last line of table 4.2. The lattice parameter a is in good agreement with the experimental data although the other lattice parameters are not well described, reflecting the poor description of Van der Waals interactions by DFT methods.

4.3.2 2D Phases

Two dimensional phases are produced at pressures from 2 to 8GPa and temperatures from 500 and 900K. Normally the two phases come together, although after a pressure of 4GPa the rhombohedral is the main phase.

The first sample of these 2D polymers was produced by Núñez-Regueiro et al. [8], using a pressure of 3GPa and a temperature of 873K. The sample was composed 65% of the rhombohedral phase and 35% of the tetragonal phase.

4.3.2.1 2D Tetragonal Phase

The tetragonal structure can be described as creating intermolecular square rings, placed between the polymeric chains in the plane defined by the a and b tetragonal axes (along two [110] cubic directions), as shown in figure 4.7(a). Figure 4.7(b) shows the crystallographic relationship between the tetragonal cell and the fcc cell from pristine C_{60}.

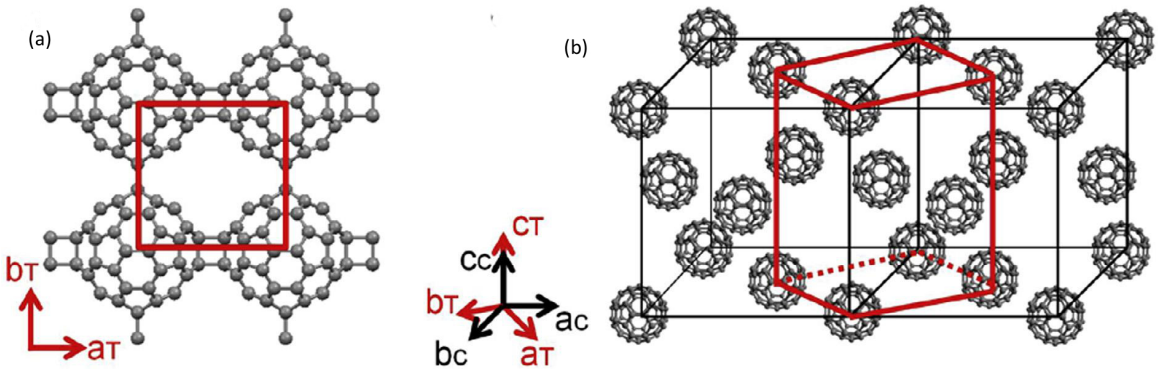

Figure 4.7: (a) Tetragonal C_{60} phase polymeric layer ascribed in tetragonal axis. (b) Relationship between the tetragonal cell and the fcc cell. Figure from [3].

The first reported 2D tetragonal structure was indexed to the orthorhombic space group $Immm$ [8], this structure is labeled as T. In this structure the polymeric stacked layers, ABAB... stacking, have the same orientation. Later Davydov et al. [45] proposed a different structure with tetragonal space group $P4_2/mmc$, the difference from the previous structure is that the B layer is rotated by 90°, about the tetragonal c axis, with respect to the A layer (this structure is labeled as T'). Later Chen and Yamanaka [9] obtained again the T structure from a single crystal sample. Table 4.3 summarizes all the data from different groups.

Table 4.3: Crystallographic data of 2D tetragonal phase for different P-T paths (P-T meaning applying first pressure then temperature and T-P in the opposite way). T-tetragonal phase, R-rhombohedral phase.

Path	Report on	Phase	space group	a(Å)	b(Å)	c(Å)	P(GPa)	T(K)	Refs.
P-T	Powder	35%T-65%R	$Immm$	9.09	9.09	14.95	3.0	873	[8]
	Powder	65%T'-35%R	$P4_2/mmc$	9.097	9.097	15.04	2.2	873	[45]
	single crystal	T	$Immm$	9.026	9.083	15.07	2.5	773	[9]
T-P	Powder	90%T'	$P4_2/mmc$	9.097	9.097	15.04	2.2	873	[45, 46]
	single crystal	75%T'-25%R dimmers	$P4_2/mmc$	9.02	9.02	14.934	2.0	700	[47, 48]
	single crystal	84%T'-16%T	84% $P4_2/mmc$ 16% $Immm$	9.064	9.064	15.039	2.2	873	[49]
	DFT	T	$Immm$	9.09	9.09	16.48	-	-	our calculations

The synthesis of phases T and T' depends on the values of pressure and temperature and also on the pressure-temperature path. If the temperature is applied before the pressure (T-P path) the rotational freedom is increased and thus the subsequent application of pressure allows the C_{60} molecules to approach close together, forming the T' phase. On the other hand if the pressure is applied first (P-T path) the molecular rotation is blocked and subsequent heating is not enough to allow molecular rotation. Nevertheless Davydov et al. [45] (second line of the table 4.3) have obtained the T' phase through the P-T path, although for the same temperature (873K) [8] they applied lower pressures (allowing more rotational freedom).

We have performed DFT calculations with VASP software on the tetragonal 2D polymeric T structure. The cell shape and volume relaxation data is presented in the last line of table 4.3. The a and b tetragonal parameters are in good agreement with the experimental data although the c parameter is in rather poor agreement. This is similar to what happens for the 1D orthorhombic phase, the lattice parameters are in good agreement when they correspond to polymeric directions while the agreement is poor for the parameters which do not correspond to polymeric directions. As stated before, this results from the poor description of the Van der Waals interactions by DFT methods.

4.3.2.2 2D Rhombohedral Phase

The rhombohedral structure can be described as creating intermolecular square rings between the polymeric chains, in the (111) fcc planes. Figures 4.8(a) and 4.8(b) show possible polymeric layers.

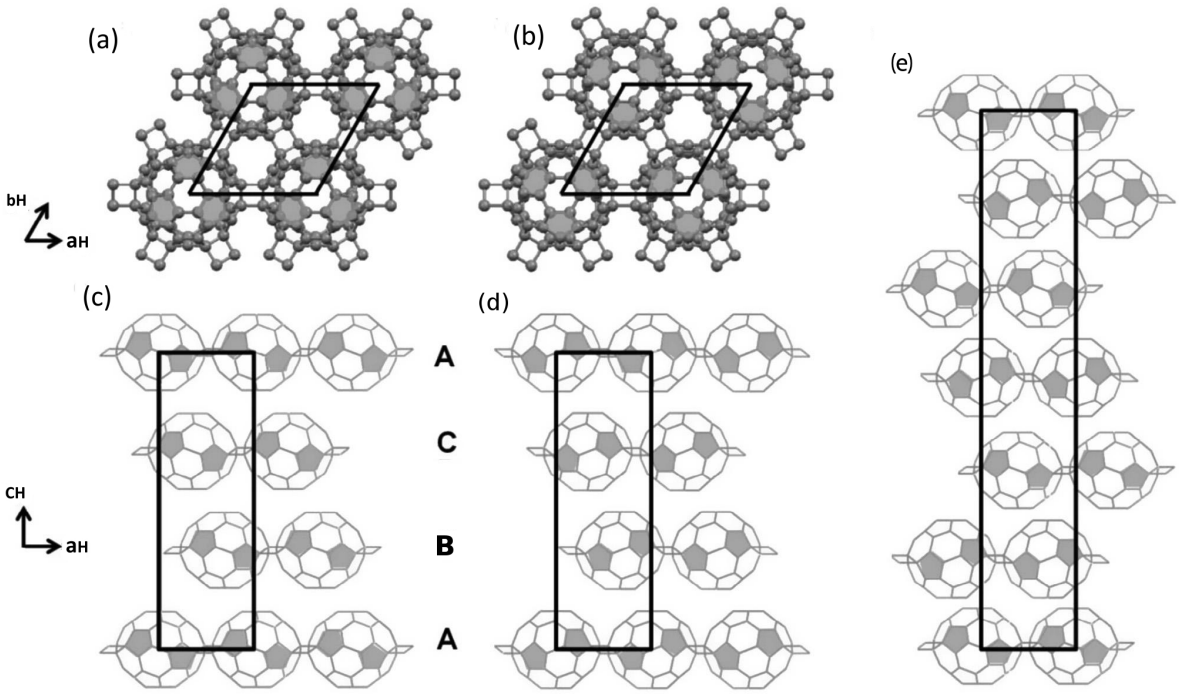

Figure 4.8: (a) Rhombohedral C_{60} phase polymeric layer. (b) Differently oriented polymeric layer. (c) ABC stacking of (a) oriented layers. (d) ABC stacking of (b) oriented layers. (e) Combined stacking model. Figure adapted from [3].

There are various proposed ways as to how the polymerized layers organize themselves. Based on their samples Nuñez-Regueiro et al. [8] proposed ABC staking, where polymerized layers have the same 4.8(a) orientation with molecules of adjacent layers facing each other

through pentagons, as seen in figure 4.8(c) (model 1). This model was confirmed by Xu and Scuseria[14], and separately by Oszlányi and Forró[50]. Based on samples from Davydov et al. [45] Dzyabchenko et al. [51] proposed a second model, figure 4.8(d) (model 2). This model is similar to the first one, the only difference is that it considers a differently oriented polymerized layers, 4.8(b), 60° rotated around the three-fold axis from the previous orientation. The molecules of adjacent layers are now facing each other through hexagons. Based on these two models Davydov et al. [52] proposed a theoretical combined model figure 4.8(e).

Table 4.4: Crystallographic data of 2D rhombohedral phase. T-tetragonal phase and R-rhombohedral phase.

Report on	Phase	space group	a(Å)	c(Å)	P(GPa)	T(K)	Refs.
Powder	R	$R\bar{3}m$	9.22	24.6	$5-7.5$	$773-1073$	[53, 54]
Powder	18%T-82%R	$R\bar{3}m$ model1	9.19	24.5	$4-5$	$873-973$	[8, 55]
single crystal	75%T-25%R dimmers	$R\bar{3}m$ model1	9.19	24.5	2.2	700	[47, 48]
Powder	R	$R\bar{3}m$ model2	9.175	24.568	6	873	[56, 57]
single crystal	R	$R\bar{3}m$ model2	9.175	24.568	5	773	[9, 58]
DFT	R	$R\bar{3}m$	9.21	26.55	-	-	our calculations

We have performed DFT calculations in the structural model 1 with VASP software. Ions cell shape and volume relaxation was made, the final lattice parameters are listed in the last line of table 4.4. We have the same situation as for 1D orthorhombic and 2D tetragonal structures: in the polymerized directions the relaxed parameters are in good agreement with the experimental data but for the parameter c, corresponding to non polymerized direction, the agreement is poor. As stated before this poor agreement comes from the poor DFT description of the Van der Waals interactions.

4.3.3 3D Cuboidal Phase

The 3D cuboidal phase is the more recent member of the family of C_{60} polymers, discovered by Yamanaka et al.[11], in 2006. It has metallic conductivity.

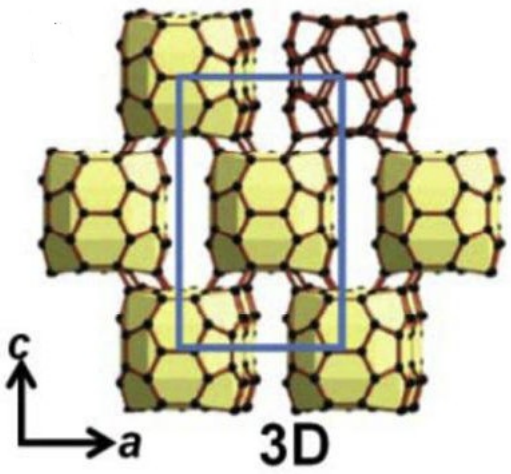

Figure 4.9: Cuboidal C_{60} phase. Figure adapted from [11].

This phase was synthesized at 15GPa and temperature up to 873K by compressing the 2D tetragonal phase. The experimental lattice parameters were $a = 7.86$Å, $b = 8.59$Å and

$c = 12.73$Å. The structure has $Immm$ space group, where C_{60} molecules are deformed into a cuboidal shape. The molecules are connected to eight nearest neighbors by (3+3) cycloaddition forming a body centered cell as shown in figure 4.9, the fullerenes in the blue rectangle vertexes are in a different plane. The intermolecular bond length is 1.41Å.

Comparing to the precursor 2D tetragonal structure, the a cell parameter strongly decreases, from around 9.1Å to around 7.86Å. Along the b parameter this decrease is also important, from 9.1Å to 8.59Å. The previous 6:6 bonds were broken along the a axis and the distance between these previously bonded atoms is 2.47Å, since they are pushed inside the C_{60} cage.

DFT studies gave optimized lattice parameters different from the experimental ones, $a = 8.581$Å, $b = 8.510$Å and $c = 13.132$Å [59]. Although the a lattice parameter is quite different the overall molecular deformation is kept. We had performed DFT studies of this phase obtaining lattice parameters of $a = 8.63$Å, $b = 8.51$Å and $c = 13.15$Å in good agreement with reference [59]. The final structure space group was also $Immm$.

Chapter 5

DFT Application

The initial DFT calculations, performed for the well known 1D, 2D and cuboidal polymeric structures (section 4.3), were made to test the PBE functional and overall DFT technique which proved to be very useful since the optimized lattice parameters are in a fair agreement with the experimental ones.

Previously to these calculation we have made a K point convergence in the Single Bond Tetragonal 3D structure, which will be described in detail in the next section 5.1. This convergence lead us to use a K points grid accordingly to Monkhorst Pack approach of $6 \times 6 \times 6$. All calculations were made with an energy cutoff of 520eV, 1.3 times the default value as recommended for calculations where cell volume is allowed to change [60]. The self-consistency cycle global energy break condition used was 10^{-5} eV. We also had to specify the break condition for the ionic loop, which was -0.01 eV. From VASP options, conjugate gradient algorithm was chosen to move the structure ions [60].

5.1 *K* Point Convergence

For convergence in the K points we made a set of self consistency cycles only changing the number of K points. We always used a $M \times M \times M$ grid of K points as it can be seen in table 5.1.

Table 5.1: Results from computing the total energy of Single Bond Tetragonal 3D structure with $M \times M \times M$ K points generated using the Monkhorst Pack method. (The time written is the time needed to make one self-consistency cycle)

M	K points in the IBZ	energy(eV)	time(s)	memory(kb)
2	8	-1054.7785	619.906	451932
3	14	-1054.7858	1016.749	691152
4	36	-1054.7770	2936.177	1569692
5	63	-1054.7778	4692.292	2658836
6	112	-1054.7778	7615.309	4636924
7	172	-1054.7778	11537.270	7051932
8	260	-1054.7778	30110.475	10614152

Looking at the third column of the table 5.1 is possible to see that using grids with M greater or equal to 5, which corresponds to use a number of K points in the IBZ greater or equal to 63, the energy per structure is the same up to the fourth decimal place. Thus it tell us that this value (after M greater or equal to 5) is not dependent on the number of K points.

To be sure that this is guaranteed we have used always a M equal to 6. Higher values would not change the solution and would increase the computational time and needed memory.

5.2 Proposed Structures and Relaxation

From the experimental diffraction pattern the 9.5GPa C_{60} polymer is known to have an fcc lattice parameter corresponding to a nearest neighbor (nn) distance of 9.33Å. Thus looking into intermolecular distances of dimers determined by theoretical methods, in section 4.2.1, the most suitable bonding configuration for this structure is through a single bond since its corresponding nn distance is 9.31Å. It has also been experimentally found that for doped C_{60} molecules are bonded by single bonds with 9.33Å nn distance [61]. We have then constructed a structure based on this bonding type with small distortion from the experimental fcc lattice.

We have also tried to construct structural models based on the molecular orientations in the same way as the low temperature simple cubic (sc) structure is obtained [4, 38, 62–64]. Starting from the four molecules of the fcc lattice in the standard orientation we rotated the same angle (comprised between 0 and 120 degrees) around a $\langle 111 \rangle$ cubic direction (each one of the four molecules was rotated around one of the four $\langle 111 \rangle$ cubic directions). We were expecting to find possible intramolecular bond alignments between molecules nn molecules, allowing intermolecular bonds to be established. No such alignments were found.

Finally we have constructed some structures based on the standard orientations because these orientations are compatible with cubic symmetry [39]. Several structures were obtained and are discussed in section 5.2.2.

The proposed structures had first their atomic position relaxed with the lattice parameters constrained to their experimental values. Then they got a full atomic, cell shape and volume relaxation at pressure conditions and finally at room conditions. In most cases the relaxation was also made directly on room conditions, as well.

5.2.1 Single Bond Tetragonal 3D Structure

Figure 5.1 shows how we can map an fcc lattice, with lattice parameter a_C, into a body centered tetragonal lattice, with parameters a_T and c_T. The relation between cubic and tetragonal parameters is as follows:

$$\begin{aligned} a_T &= \frac{a_C}{\sqrt{2}} \\ c_T &= a_C \end{aligned} \tag{5.1}$$

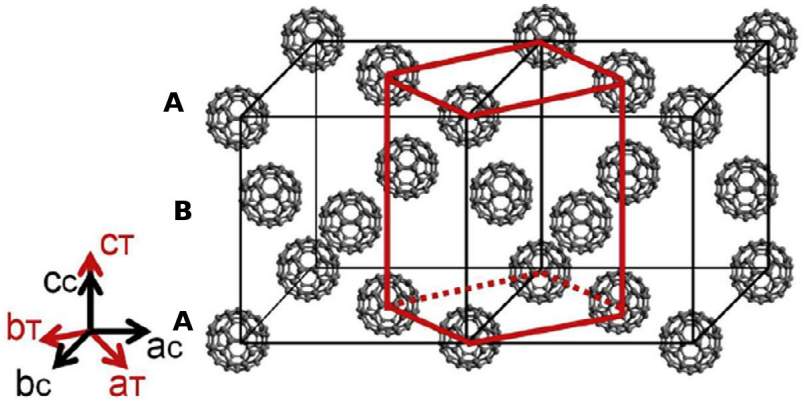

Figure 5.1: Relationship between the tetragonal cell and the fcc cell. It is also shown an AB stacking of (001) planes. Figure adapted from [3].

To construct the single bond tetragonal structure we have considered the AB stacking of the (001) planes in an fcc lattice, as shown in figure 5.1. In the A layer the molecules have the standard orientation S while molecules in the B layer have the S' standard orientation. Then both molecules were rotated around 27.5° with respect to the [001] direction, in order to have atoms from molecules in the A layer facing atoms in the molecules of the adjacent B layers. The molecules were kept undeformed excepting the atoms pointing towards the nn molecules, which were pulled out ≈ 0.3Å in order to have intermolecular covalent distances of $\approx$1.5Å. The resulting structure has two molecules per primitive cell and it belongs to $P4_2/m$ tetragonal space group. The lattice parameters were constrained to a distortion around 1% from the experimental fcc lattice parameters.

The relaxed structure is shown in figure 5.2, and a network scheme of such structure is displayed in 5.3. After relaxation the polymeric single bonds are kept between molecules of adjacent (001) planes. No bonds are formed within the (001) planes. Each molecule is bonded to 8 nearest nn molecules in the adjacent (001) planes, as shown in schematically in figure 5.3

Single Bond Tetragonal 3D structure has proven to be stable. The structure full relaxation (atomic, cell shape and volume relaxation) yielded lattice parameters of $a_T = 9.56$Å and $c_T = 12.88$Å at room conditions giving a bonding nn distance of 9.34Å (between molecules in different (001) planes) and non bonding nn distance of $a_T = 9.56$Å (molecules in the same (001) plane). The $P4_2/m$ symmetry was kept. Although the bonded nn distance is in good agreement with experimental data, the cell distortion is inconsistent with the same data, having a c_T/a_T cell distortion (≈ 1.3) smaller than the one admitted by a cubic symmetry ($\sqrt{2}$) and must be discarded as the structure for the 9.5GPa C_{60} polymer, and it will not be discussed further.

Table 5.2: Fractional atomic coordinates of Single Bond Tetragonal 3D structure after ionic, cell shape and volume relaxation at room conditions (left) and at 9.5GPa (right), and lattice parameters after and before relaxation.

	room conditions				9.5GPa		
atom	x	y	z		x	y	z
C(1)	0.06525	-0.46454	-0.26897		0.06674	-0.46343	0.22669
C(2)	0.16942	0.18483	-0.05498		0.17455	0.17290	0.44435
C(3)	0.35116	-0.39175	0.00000		-0.38996	-0.36144	0.00000
C(4)	0.28263	-0.26031	0.00000		-0.25340	-0.29242	0.00000
C(5)	0.19007	0.46606	-0.23607		0.19375	0.46543	0.26258
C(6)	0.07132	-0.31980	0.23650		0.07232	-0.31648	-0.26263
C(7)	0.25567	0.28067	-0.11034		0.26244	0.27314	0.38913
C(8)	-0.04121	-0.16723	0.11126		-0.04166	-0.15655	-0.38792
C(9)	-0.20908	0.21568	-0.09101		-0.21600	0.20736	0.40845
C(10)	-0.34581	0.47872	-0.09125		-0.35656	0.48000	0.40796
C(11)	0.27451	-0.43707	-0.18142		0.28110	-0.43706	0.31762
C(12)	0.21766	-0.28830	0.19350		0.22156	-0.28540	-0.30629
C(13)	0.19535	0.31032	-0.21710		0.19816	0.30673	0.28234
C(14)	-0.04733	-0.25111	0.20425		-0.04782	-0.24445	-0.29501
C(15)	0.33382	0.37753	-0.05595		0.34430	0.37193	0.44350
C(16)	-0.08532	0.15024	0.05700		-0.08921	0.13870	-0.44240
lattice parameters	a(Å)	b(Å)	c(Å)		a(Å)	b(Å)	c(Å)
after relaxation	9.56	9.56	12.88		9.24	9.24	12.65
before relaxation	9.38	9.38	13.13		9.01	9.01	12.74

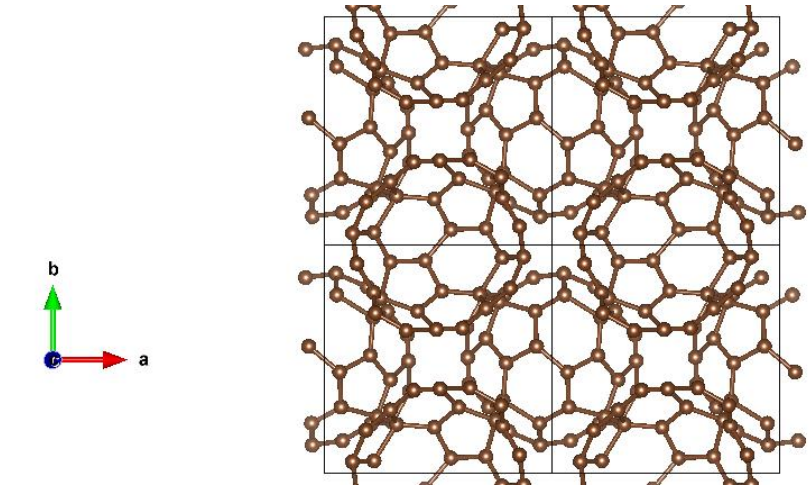

(a)

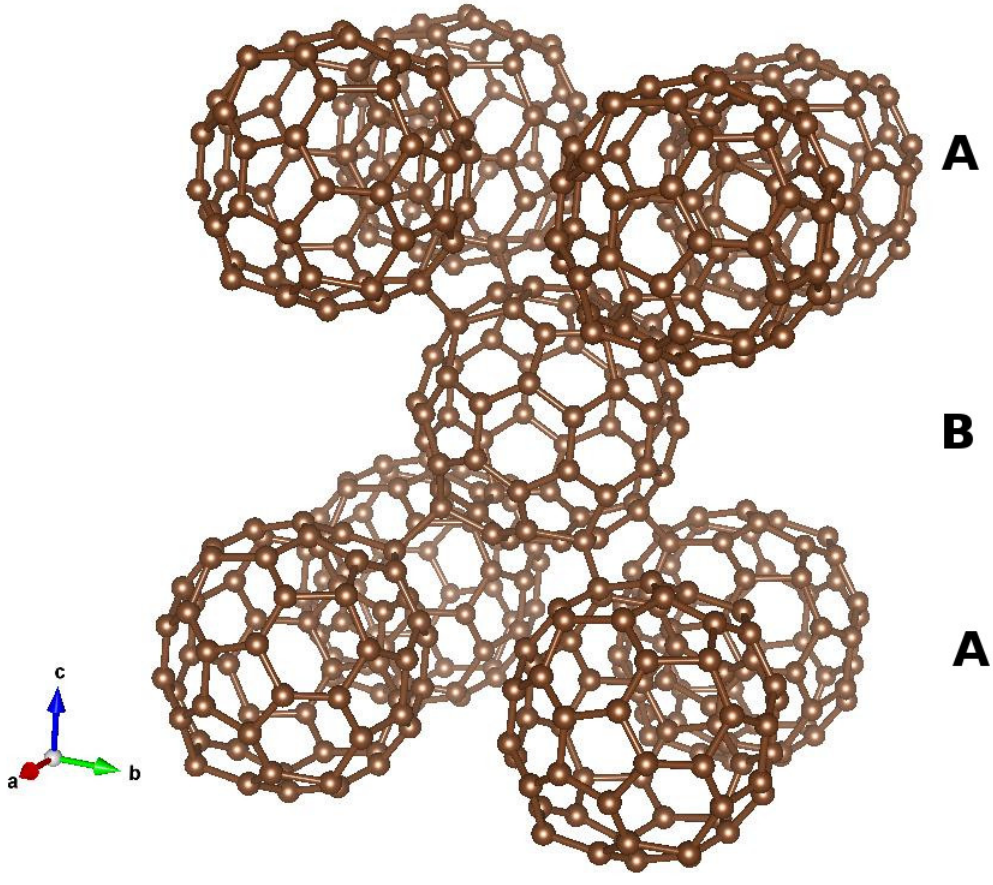

(b)

Figure 5.2: Single Bond Tetragonal 3D structure. (a) Single Bond Tetragonal 3D structure perpendicular to an (a, b) plane. (b) Single Bond Tetragonal 3D structure in perspective.

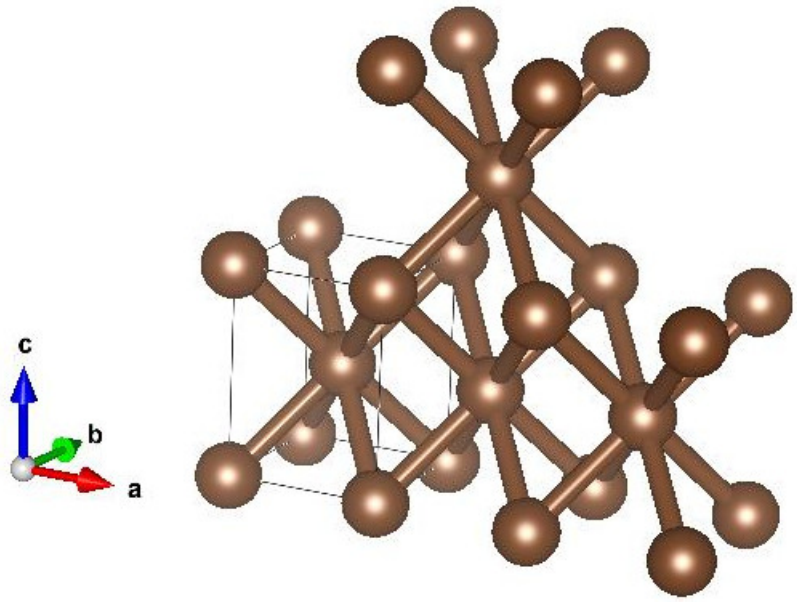

Figure 5.3: Single Bond Tetragonal 3D bonding scheme.

We have also studied the structure where molecules of A and B (001) planes have the same orientation. This structure belongs to the monoclinic $C2/m$ space group. After relaxation this structure proved to be unstable since, the 3D bonds network between molecules was lost with each molecule keeping just four polymeric nn bonds instead of the initial eight. A 2D polymerized structure was then obtained.

As the Single Bond Tetragonal 3D structure failed to describe the experimental data we turn our attention to structures based on combinations of the molecular standard orientations, described in section 4.1.1, constrained to a cubic metric.

5.2.2 Structures with Standard Molecular Orientations

Structures with molecules having standard orientations were constructed. In these starting structures the molecules are undeformed, excepting the two atoms pointing to the nn molecule (with the same and different standard orientation) which were pulled out ≈ 0.3Å in order to have a covalent distance of ≈ 1.5Å between the atoms of nn molecules.

In an initial stage an fcc structure, space group $Fm\bar{3}$, with all molecules having the same standard orientation was considered. All bonds were lost after an atomic, cell shape and volume full relaxation. The lattice parameter has relaxed to 14.79Å from an initial value of 13.15Å.

5.2.2.1 $P4_2/mnm$ Structure

In this structure we consider an AB stacking of the (001) planes in an fcc lattice. The A layer have molecules with S standard orientation while the B layer have molecules with S' standard orientation, as seen in figure 5.4. In figure 5.5(a) it is easily seen the four-fold screw axis along the [001] direction. This structure belongs to $P4_2/mnm$ tetragonal space group.

$P4_2/mnm$ structure is stable under DFT calculations. The relaxed structure is shown in figure 5.5(b). Bonds between nn molecules of the same plane, with the same orientation, are lost and bonds between nn molecules of different planes, with opposite orientations, are kept.

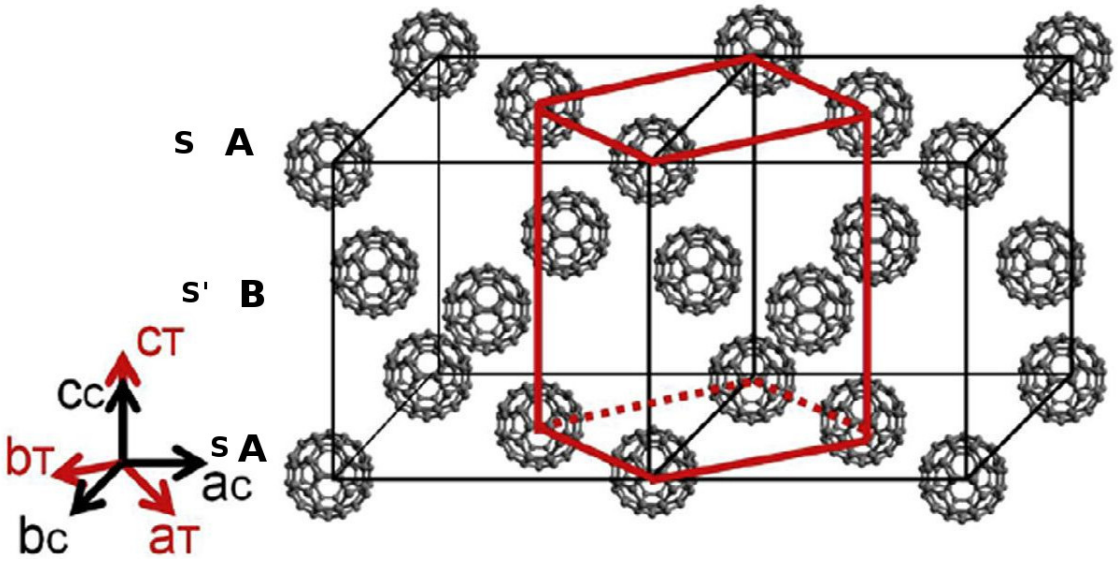

Figure 5.4: Relationship between the tetragonal cell and the fcc cell. It is also shown the AB stacking of (001) planes and correspondent standard orientation of each plane. Figure adapted from [3].

In this way each molecule will be bonded to eight nn molecules, four from the plane above and other four from the plane below, through a (2+2) cycloaddition 5:6(PP-SS).

After full relaxation the lattice parameters had values of $a_T = 9.32$Å, $c_T = 12.87$Å at room conditions. $P4_2/mnm$ space group was kept. The molecular center to center distance between bonding nn is 9.21Å having now a smaller value than $a_T = 9.32$ that is the distance between non bonding nn molecules. Table 5.3 shows the fractional coordinates and lattice parameters of the final structure relaxed under pressure and at room conditions.

Table 5.3: Fractional atomic coordinates of $P4_2/mnm$ structure after ionic, cell shape and volume relaxation at room conditions (left) and at 9.5GPa (right), and lattice parameters after and before relaxation.

	room conditions				9.5GPa		
atom	x	y	z		x	y	z
C(1)	-0.44444	-0.44444	0.24578		-0.44366	-0.44366	0.24294
C(2)	0.25711	0.25711	0.05548		0.26543	0.26543	0.05583
C(3)	0.31908	-0.21062	0.00000		-0.17299	-0.28390	0.50000
C(4)	-0.29941	-0.47775	0.26428		-0.29695	-0.47742	0.26449
C(5)	-0.18691	0.36119	0.38881		-0.17901	0.35709	0.38860
C(6)	-0.16263	-0.37503	0.40900		-0.15543	-0.37243	0.40886
C(7)	-0.22279	-0.34376	0.30460		-0.21953	-0.34249	0.30524
C(8)	-0.25081	0.37169	0.28120		-0.24820	0.37078	0.28213
C(9)	-0.14299	0.48167	0.44361		-0.13652	0.48100	0.44352
lattice parameters	a(Å)	b(Å)	c(Å)		a(Å)	b(Å)	c(Å)
after relaxation	9.32	9.32	12.87		9.07	9.07	12.72
before relaxation	9.33	9.33	13.20		9.01	9.01	12.74

The relaxed structure nn intermolecular distance (9.26Å) is shorter than the experimental

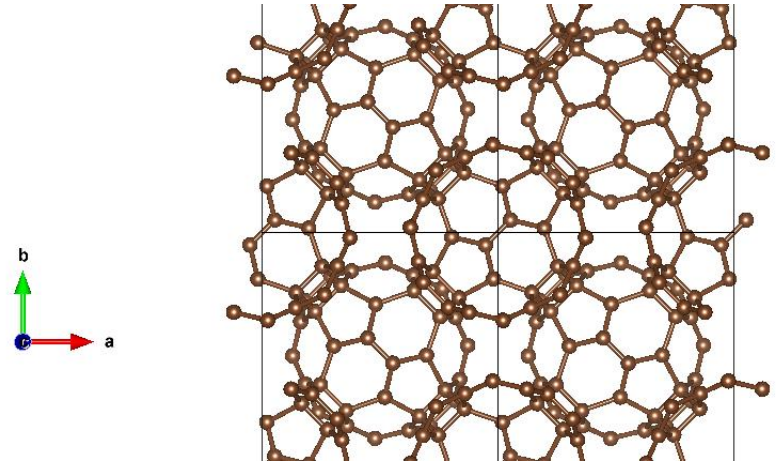

(a)

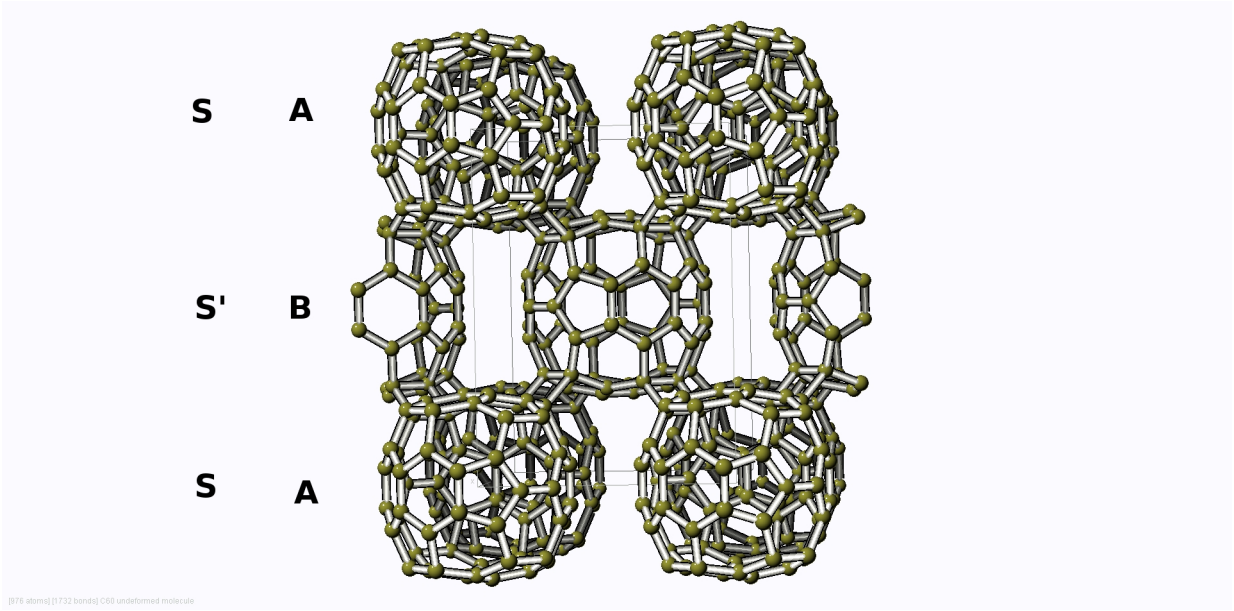

(b)

Figure 5.5: $P4_2/mnm$ structure. (a) $P4_2/mnm$ structure perpendicular to an (a, b) plane. (b) The $P4_2/mnm$ structure in perspective.

---

one (9.33Å) and the cell presents a distortion which is inconsistent with the same data, having a ratio $c_T/a_T = 1.38$ smaller than the one admitted by an fcc cell ($\sqrt{2}$), thus loosing the initial cubic metric. Thus, this structure must be discarded as the structure of the 9.5GPa C_{60} polymer.

5.2.2.2 $R\bar{3}c$ Structure

In this structure the molecules alternating the (111) cubic planes have different standard orientations. We consider an AB'CA'BC' stacking along the [111] cubic direction, as defined in figure 5.6. The A, B and C layers have molecules with S orientation and the A', B' and C' layer have molecules with S' orientation. This structure belongs to $R\bar{3}c$ rhombohedral space group. From figure 5.7 it is easily seen the 3-fold rotation axis of the obtained structure.

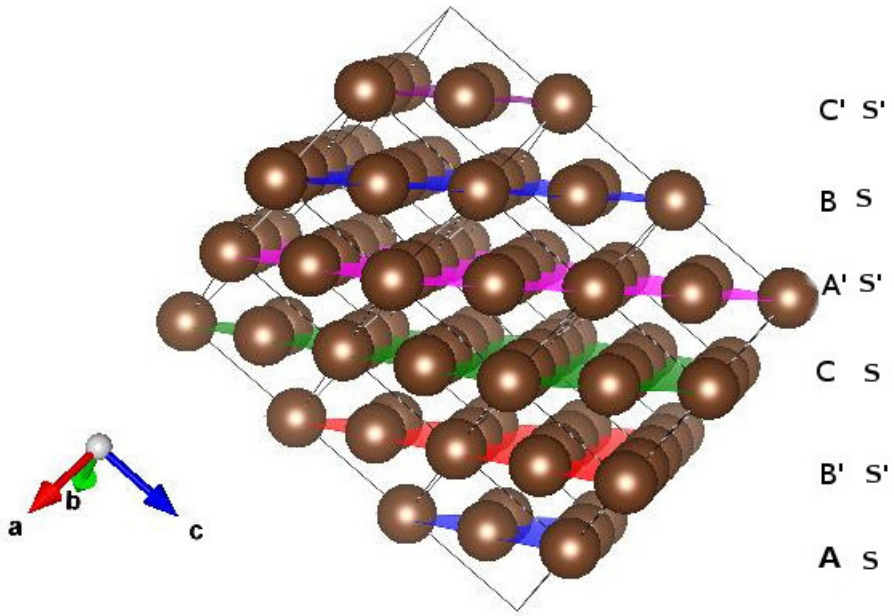

Figure 5.6: AB'CA'BC' stacking along the [111] cubic direction.

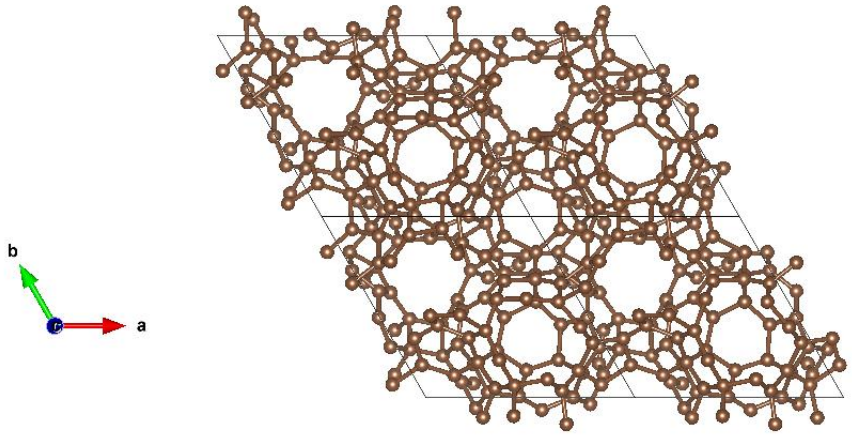

Figure 5.7: $R\bar{3}c$ structure seen along c hexagonal axis.

$R\bar{3}c$ structure is stable after DFT relaxation. Bonds between nn molecules of the same plane, with the same orientation, are lost and bonds between nn molecules of different planes, with different orientations, are kept. In this way, each molecule will bond to six nn molecules, three from the plane above and three from the plane below, through a (2+2) cycloaddition 5:6(PP-SS). The bonding scheme is shown in figure 5.8.

After full relaxation the hexagonal lattice parameters had values of $a_H = 9.52$Å, $c_H = 44.70$Å at room conditions. $R\bar{3}c$ space group was kept. The molecular center to center distance between bonding nn is 9.26Å having a smaller value than $a_H = 9.52$ that is the distance between non bonding nn molecules. Table 5.3 show the fractional coordinates and lattice parameters of the final structure relaxed under pressure and at room pressure.

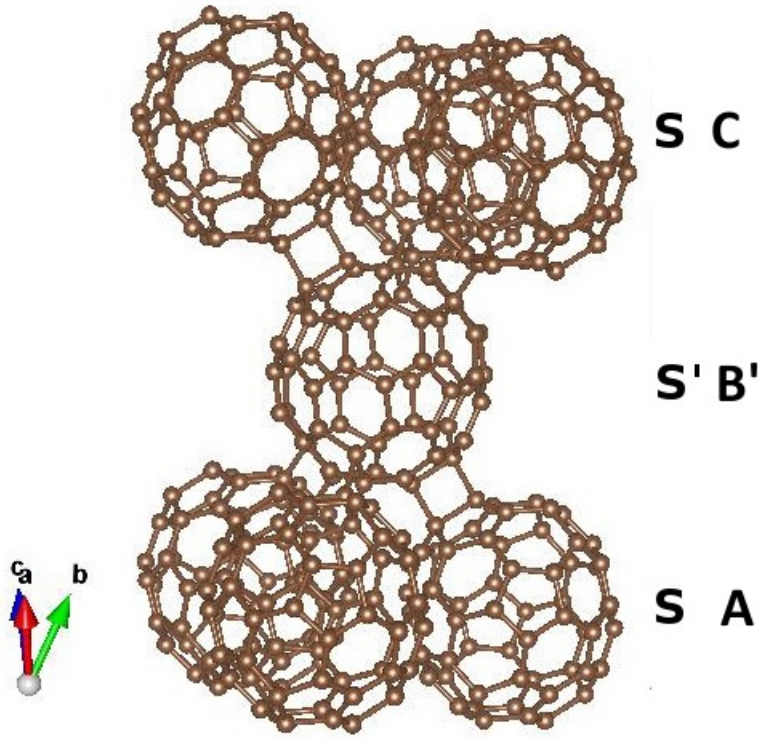

Figure 5.8: The relaxed $R\bar{3}c$ structure seen in perspective.

Table 5.4: Fractional atomic coordinates of $R\bar{3}c$ structure after ionic, cell shape and volume relaxation at room conditions (left) and at 9.5GPa (right), and lattice parameters after and before relaxation.

	room conditions				9.5GPa		
atom	x	y	z		x	y	z
C(1)	-0.29835	-0.21593	0.20223		0.38462	0.12785	0.03613
C(2)	-0.49425	-0.23340	0.24144		0.17723	0.10514	0.07455
C(3)	-0.24363	-0.15471	0.17239		0.43740	0.18988	0.00585
C(4)	-0.36297	-0.38463	0.20214		0.31592	-0.04643	0.03577
C(5)	-0.37651	-0.00595	0.20932		0.29718	0.33982	0.04301
C(6)	0.41190	-0.14309	0.24722		0.07550	0.19082	0.07999
C(7)	0.49315	0.01303	0.22492		0.15811	0.35206	0.05826
C(8)	-0.32915	0.04537	0.18036		0.34378	0.39215	0.01372
C(9)	0.43432	0.07271	0.17207		0.09800	0.41571	0.00545
C(10)	-0.37050	-0.14482	0.22078		0.30829	0.19991	0.05467
lattice parameters	a(Å)	b(Å)	c(Å)		a(Å)	b(Å)	c(Å)
after relaxation	9.52	9.52	44.70		9.19	9.19	44.02
before relaxation	-	-	-		9.01	9.01	44.14

The center to center distance between bonded nn molecules in the relaxed structure is shorter than the experimental one (9.33Å) and the cell presents a distortion which is inconsistent with the fcc experimental data. There was a cell distortion from the initial cubic metric to a rhombohedral metric that can be seen as an approximation of the (111) planes, which make us exclude this structure as the structure of the 9.5GPa C_{60} polymer.

5.2.2.3 $Pm\bar{3}$ Structure

This structure belongs to $Pm\bar{3}$ cubic space group. The molecules on the corners of the unit cell have S orientation while those on the faces have the S' orientation. Hence, we have a ratio of one S molecule to three S' molecules.

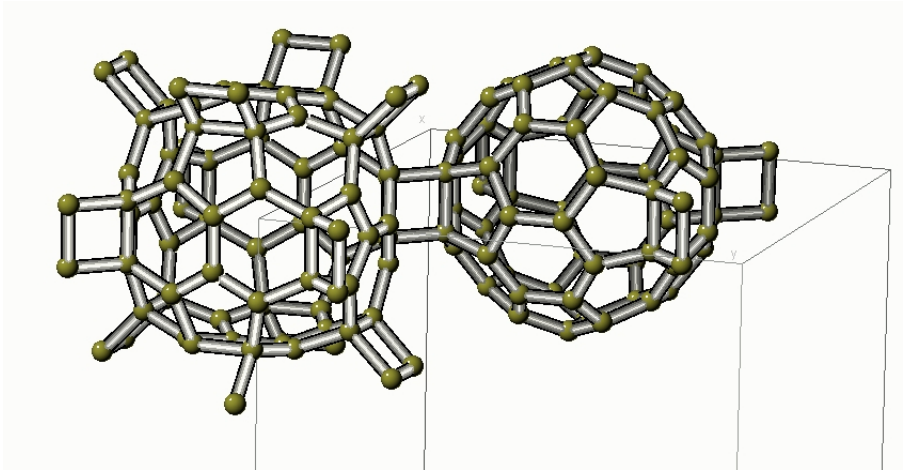

(a)

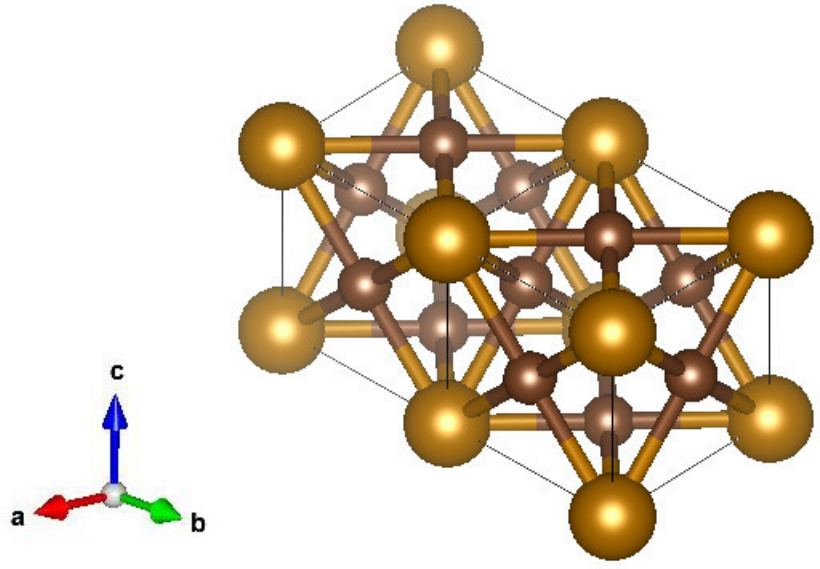

(b)

Figure 5.9: $Pm\bar{3}$ structure. (a) Molecule belonging to the unit cell corner S (left) and S'(right) oriented molecule belonging the unit cell face, after relaxation. (b) Bonding scheme of $Pm\bar{3}$ structure after relaxation, bigger yellow spheres represent the S orientation molecules and the smaller brown spheres represent S' orientation molecules.

After full relaxation, and in agreement with the previous structures, bonds between molecules having the same orientation broke while bonds between molecules differently oriented were kept. The molecules in the corners of the unit cell are bonded to twelve nn molecules while molecules on the faces are bonded only to four nn molecules. This bonding scheme is shown in figure 5.9(b). The different bonding in differently oriented molecules may be seen in figure 5.9(a).

Relaxing the structure to ambient conditions from high pressures give a lattice parameter $a_c = 13.15$Å in quite good agreement with the experimental value. A nn distance of 9.30Å characterizes this structure in both bonded and non bonded directions.

Although this structure has good agreement with the experimental data we shall notice some adversities caused by the asymmetric ratio between S and S' orientations:

- Polymerization in C_{60} molecules is known to start by forming dimers. This means that in the present case the dimers are formed between molecules with different standard orientations implying a ratio of nearly 1:1 instead of the present 3:1.
- This structure is simple cubic and thus its diffraction pattern should display superlattice reflections which are not observed.

Table 5.5: Fractional atomic coordinates of $Pm\bar{3}$ structure after ionic, cell shape and volume relaxation at room conditions (left) and at 9.5GPa (right), and lattice parameters after and before relaxation.

	room conditions				9.5GPa		
atom	x	y	z		x	y	z
C(1)	0.00000	0.05514	0.24443		0.00000	0.05582	0.25099
C(2)	0.22860	-0.08973	0.11085		0.23189	-0.09051	0.11196
C(3)	0.21697	-0.19159	0.06143		0.21814	-0.19225	0.06189
C(4)	0.00000	-0.23943	0.44512		0.00000	-0.23366	0.44439
C(5)	0.50000	0.26292	-0.44628		0.50000	0.27121	-0.44502
C(6)	0.50000	0.23432	0.05427		0.50000	0.22990	0.05548
C(7)	0.26856	0.38910	0.08769		0.26489	0.38813	0.08925
C(8)	-0.39304	-0.41237	0.22638		-0.39098	-0.41122	0.23228
C(9)	-0.41030	-0.26797	0.10641		-0.40966	-0.26548	0.10844
C(10)	0.30754	0.28239	0.06064		0.30679	0.28148	0.06155
C(11)	-0.30489	-0.44534	0.16915		-0.30191	-0.44458	0.17268
C(12)	-0.44497	-0.32770	0.18985		-0.44423	-0.32616	0.19362
lattice parameters	a(Å)	b(Å)	c(Å)		a(Å)	b(Å)	c(Å)
after relaxation	13.15	13.15	13.15		12.85	12.85	12.85
before relaxation	-	-	-		12.74	12.74	12.74

Chapter 6

Discussion and Conclusions

The previously DFT optimized structures are not suitable to describe the 9.5GPa C_{60} phase because they show distortions incompatible with the observed cubic lattice. The $Pm\bar{3}$ structure having cubic symmetry is discarded by the reasons mentioned before. However, DFT results give us the clues to find the 9.5GPa C_{60} polymeric structure.

In these structures polymeric bonding occurs between molecules with different orientations, S and S', and thus it is analogous to the antiferromagnetic bonding. S may be ascribed to an up or plus spin and S' to a down or minus spin. Since the number of S molecules is equal to the number of S' molecules, our system can be mapped to the antiferromagnetic Ising model with nn interactions. This model has other applications, besides magnetism, such as binary alloys and orientational glasses.

The antiferromagnetic Ising model with nn interactions in an fcc lattice is a classical case of frustration. The antiferromagnetic interactions cannot be fully satisfied (see illustration of frustrated antiferromagnetic interactions in a triangular lattice and in a tetrahedron shown in figure 6.1). Thus, the novel 9.5GPa phase, having an fcc lattice, should have a frustrated structure, because it is not possible for one molecule to be bonded to its twelve nn molecules in that lattice type. One way to avoid frustration and creating ordered structures is by decreasing the symmetry, as is the case of the antiferromagnetic MnO [65].

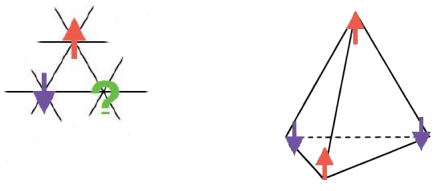

(a) (b)

Figure 6.1: (a) Frustration in a triangular lattice. (b) Frustration in a tetrahedron.

Danielian [66] calculated the number of ground state configurations for the antiferromagnetic Ising model with nn interactions in an fcc lattice, one of such ground state configurations is schematically shown in 6.2(a). In the ground state each site have eight antiferromagnetic bonds and four non-desirable ferromagnetic bonds. Mapping this configuration to the polymeric 9.5GPa C_{60}, the bonding pattern is shown schematically in figure 6.2(b) in which each molecule is bonded to eight nn out of twelve. The bonding pattern obtained is extended in the 3D space and, thus, is a 3D C_{60} polymer.

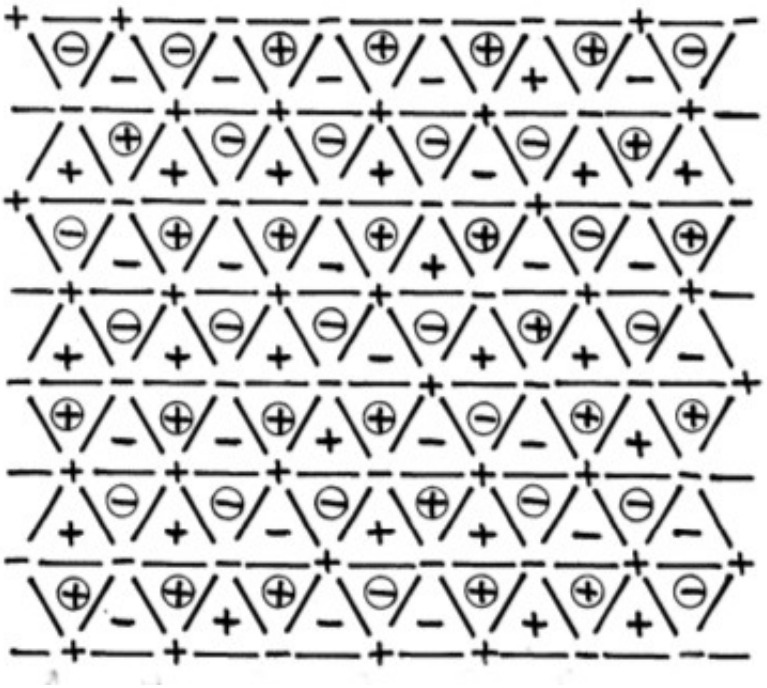

(a)

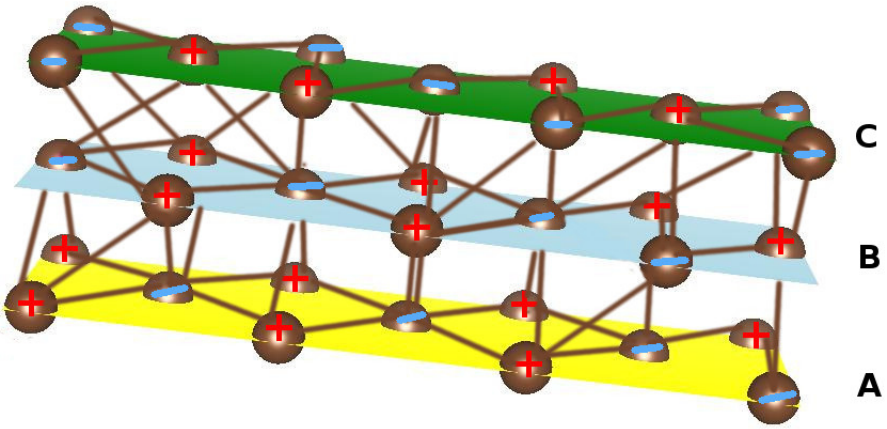

(b)

Figure 6.2: Antiferromagnetic order of spins in an fcc structure after Danielian [66]. (a) Layer one are the sites in the triangle vertexes, layer two are the site inside the circles, layer three are the sites in the triangle faces. (b) 3D polymeric bonding for the frustrated structure corresponding to the ground state configuration (a).

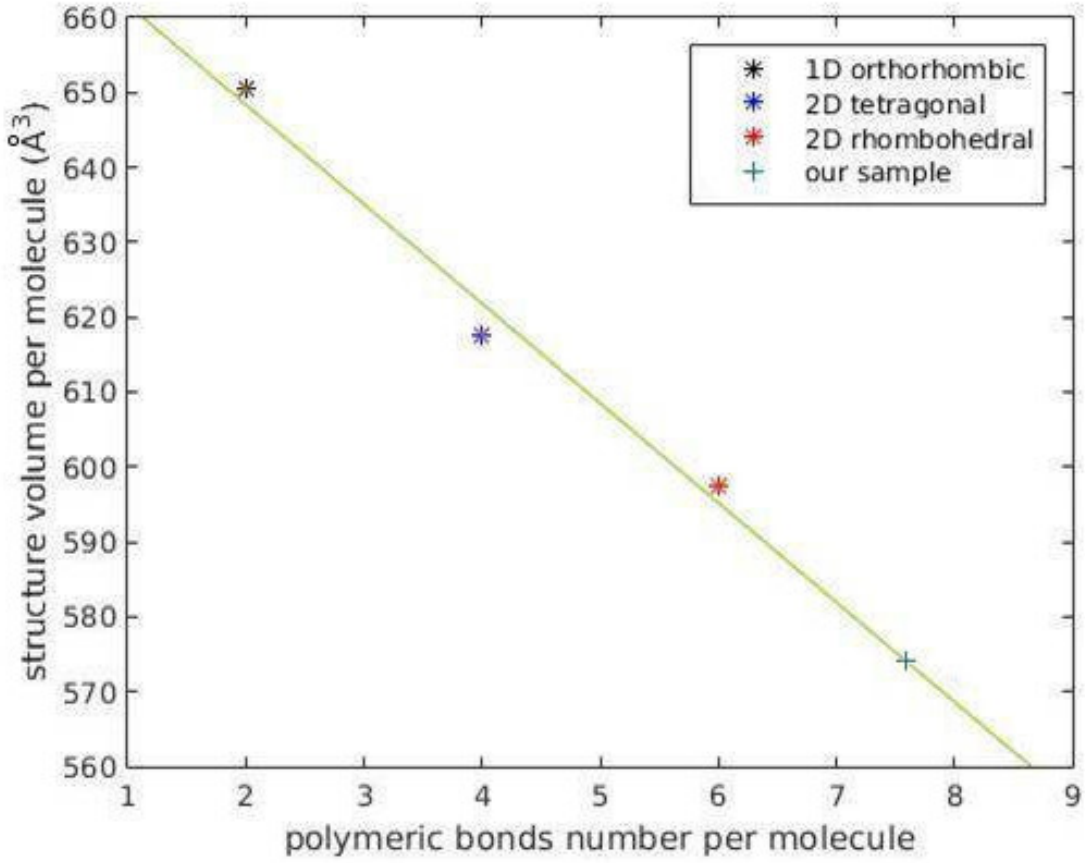

Figure 6.3: Plot of known 1D and 2D structures available volume per molecule in function of the number of formed polymeric bonds (square rings) per molecule and its linear regression.

Plotting the volume per molecule against the number of polymeric bonds for the known 1D and 2D polymer structures, an approximate linear relation is obtained, shown in figure 6.3. In the new phase, each molecule has an available volume of 574Å^3 and, thus, the corresponding number of polymeric bonds is close to eight, as Talyzin et al. [68] previously noted, in a striking agreement with the frustrated structural model for the C_{60} polymer shown in 6.2(b). Hence our structure must be a case of bonding frustration in an fcc lattice.

In conclusion, DFT calculations have been used to check the stability and to optimize C_{60} polymeric structures. This method has proved to be an important tool in the discovery of new structures, complementing experimental x-ray diffraction data when only low resolution data is available. From our DFT calculations, a frustrated structure, based on 5:6(PP) bonding, was proposed for the 9.5GPa polymeric phase. The strategy used here may also be applied to find the structures of others 3D C_{60} polymers which have remained unknown for years.

Bibliography

[1] H. W. Kroto, J. R. Heath, S. C. O'Brien, R. F. Curl, and R. E. Smalley. C_{60}: Buckminsterfullerene. *Nature*, 318:162–163, 1985.

[2] W. Krätschmer, L. D. Lamb, K. Fostiropoulos, and D. R. Huffman. Solid C_{60}: a new form of carbon. *Nature*, 347:354–358, 1990.

[3] M. Álvarez−Murga and J.L. Hodeau. Structural phase transitions of C_{60} under high-pressure and high-temperature. *Carbon*, 82:381 – 407, 2015.

[4] P. A. Heiney. Structure, dynamics and ordering transition of solid C_{60}. *Journal of Physics and Chemistry of Solids*, 53:1333 – 1352, 1992.

[5] A. M. Rao, P. Zhou, K.-A. Wang, G. T. Hager, J. M. Holden, Y. Wang, W.-T. Lee, X.-X. Bi, P. C. Eklund, D. S. Cornett, M. A. Duncan, and I. J. Amster. Photoinduced polymerization of solid C_{60} films. *Science*, 259:955–957, 1993.

[6] Y. Iwasa, T. Arima, R. M. Fleming, T. Siegrist, O. Zhou, R. C. Haddon, L. J. Rothberg, K. B. Lyons, H. L. Carter, A. F. Hebard, R. Tycko, G. Dabbagh, J. J. Krajewski, G. A. Thomas, and T. Yagi. New phases of C_{60} synthesized at high pressure. *Science*, 264:1570–1572, 1994.

[7] V. Agafonov, V. A. Davydov, L. S. Kashevarova, A. V. Rakhmanina, A. Kahn-Harari, P. Dubois, R. Céolin, and H. Szwarc. 'low-pressure' orthorhombic phase formed from pressure-treated C_{60}. *Chemical Physics Letters*, 267:193 – 198, 1997.

[8] M. Núñez−Regueiro, L. Marques, J L. Hodeau, O. Béthoux, and M. Perroux. Polymerized fullerite structures. *Phys. Rev. Lett.*, 74:278–281, 1995.

[9] X. Chen and S. Yamanaka. Single-crystal x-ray structural refinement of the 'tetragonal' C_{60} polymer. *Chemical Physics Letters*, 360:501 – 508, 2002.

[10] X. Chen, S. Yamanaka, K. Sako, Y. Inoue, and M. Yasukawa. First single-crystal x-ray structural refinement of the rhombohedral C_{60} polymer. *Chemical Physics Letters*, 356:291 – 297, 2002.

[11] S. Yamanaka, A. Kubo, K. Inumaru, K. Komaguchi, N. S. Kini, T. Inoue, and T. Irifune. Electron conductive three-dimensional polymer of cuboidal C_{60}. *Phys. Rev. Lett.*, 96:076602, 2006.

[12] S. Okada and S. Saito. Rhombohedral C_{60} polymer: A semiconducting solid carbon structure. *Phys. Rev. B*, 55:4039–4041, 1997.

[13] S. Okada and S. Saito. Electronic structure and energetics of pressure-induced two-dimensional C_{60} polymers. *Phys. Rev. B*, 59:1930–1936, 1999.

[14] C. H. Xu and G. E. Scuseria. Theoretical predictions for a two-dimensional rhombohedral phase of solid C_{60}. *Phys. Rev. Lett.*, 74:274–277, 1995.

[15] Y. Yamagami and S. Saito. Polymerized sp^2-sp^3 hybrid metallic phase of C_{60} as obtained via constant-pressure molecular dynamics. *Phys. Rev. B*, 79:045425, 2009.

[16] G. E. Scuseria. What is the lowest-energy isomer of the C_{60} dimer? *Chemical Physics Letters*, 257:583 – 586, 1996.

[17] G. Kresse and J. Hafner. *Ab initio* molecular dynamics for liquid metals. *Phys. Rev. B*, 47:558–561, 1993.

[18] G. Kresse and J. Hafner. *Ab initio* molecular-dynamics simulation of the liquid-metal–amorphous-semiconductor transition in germanium. *Phys. Rev. B*, 49:14251–14269, 1994.

[19] G. Kresse and J. Furthmüller. Efficiency of ab-initio total energy calculations for metals and semiconductors using a plane-wave basis set. *Comput. Mater. Sci.*, 6:15 – 50, 1996.

[20] G. Kresse and J. Furthmüller. Efficient iterative schemes for ab initio total-energy calculations using a plane-wave basis set. *Phys. Rev. B*, 54:11169–11186, 1996.

[21] A. R. Oganov and C. W. Glass. Crystal structure prediction using ab initio evolutionary techniques: Principles and applications. *The Journal of Chemical Physics*, 124:244704, 2006.

[22] A. R. Oganov, A. O. Lyakhov, and M. Valle. How evolutionary crystal structure prediction works—and why. *Accounts of Chemical Research*, 44:227–237, 2011.

[23] A. O. Lyakhov, A. R. Oganov, H. T. Stokes, and Q. Zhu. New developments in evolutionary structure prediction algorithm uspex. *Computer Physics Communications*, 184:1172 – 1182, 2013.

[24] C. W. Glass, A. R. Oganov, and N. Hansen. Uspex—evolutionary crystal structure prediction. *Computer Physics Communications*, 175:713 – 720, 2006.

[25] A. R. Oganov and C. W. Glass. Evolutionary crystal structure prediction as a tool in materials design. *Journal of Physics: Condensed Matter*, 20:064210, 2008.

[26] K. Momma and F. Izumi. *VESTA3* for three-dimensional visualization of crystal, volumetric and morphology data. *Journal of Applied Crystallography*, 44:1272–1276, 2011.

[27] J. M. Besson, G. Hamel, T. Grima, R. J. Nelmes, J. S. Loveday, S. Hull, and D. Häusermann. A large volume pressure cell for high temperatures. *High Pressure Research*, 8:625–630, 1992.

[28] K. Capelle. A bird's-eye view of density-functional theory. *Brazilian Journal of Physics*, 36:1318, 2006.

[29] P. E. Blöchl. Projector augmented-wave method. *Phys. Rev. B*, 50:17953–17979, 1994.

[30] H. J. Monkhorst and J. D. Pack. Special points for brillouin-zone integrations. *Phys. Rev. B*, 13:5188–5192, 1976.

[31] D. Sholl and J. A. Steckel. *Density Functional Theory: A Practical Introduction*. Wiley, 2009.

[32] J. P. Perdew, K. Burke, and M. Ernzerhof. Generalized gradient approximation made simple. *Phys. Rev. Lett.*, 77:3865–3868, 1996.

[33] J. P. Perdew, K. Burke, and M. Ernzerhof. Erratum: Generalized gradient approximation made simple. *Phys. Rev. Lett.*, 78:1396–1396, 1997.

[34] V. Milman, B. Winkler, J. A. White, C. J. Pickard, M. C. Payne, E. V. Akhmatskaya, and R. H. Nobes. Electronic structure, properties, and phase stability of inorganic crystals: A pseudopotential plane-wave study. *International Journal of Quantum Chemistry*, 77:895–910, 2000.

[35] P. H. T. Philipsen and E. J. Baerends. Relativistic calculations to assess the ability of the generalized gradient approximation to reproduce trends in cohesive properties of solids. *Phys. Rev. B*, 61:1773–1778, 2000.

[36] B. Hammer, L. B. Hansen, and J. K. Nørskov. Improved adsorption energetics within density-functional theory using revised perdew-burke-ernzerhof functionals. *Phys. Rev. B*, 59:7413–7421, 1999.

[37] M. Fuchs, J. L. F. Da Silva, C. Stampfl, J. Neugebauer, and M. Scheffler. Cohesive properties of group-iii nitrides: A comparative study of all-electron and pseudopotential calculations using the generalized gradient approximation. *Phys. Rev. B*, 65:245212, 2002.

[38] A. B. Harris and R. Sachidanandam. Orientational ordering of icosahedra in solid C_{60}. *Phys. Rev. B*, 46:4944–4957, 1992.

[39] R. M. Fleming, T. Siegrist, P. M. Marsh, B. Hessen, A. R. Kortan, D. W. Murphy, R. C. Haddon, R. Tycko, G. Dabbagh, A. M. Mujsce, and et al. Diffraction symmetry in crystalline, close-packed C_{60}. *MRS Proceedings*, 206, 1990.

[40] V. A. Davydov, L. S. Kashevarova, A. V. Rakhmanina, V. M. Senyavin, O. P. Pronina, N. N. Oleynikov, V. Agafonov, R. Céolin, H. Allouchi, and H. Szwarc. Pressure-induced dimerization of fullerene C_{60}: a kinetic study. *Chemical Physics Letters*, 333:224 – 229, 2001.

[41] J. D. Coyle. *Introduction to Organic Photochemistry*. Wiley, 1986.

[42] M. J. Frisch, G. W. Trucks, H. B. Schlegel, G. E. Scuseria, M. A. Robb, J. R. Cheeseman, G. Scalmani, V. Barone, G. A. Petersson, H. Nakatsuji, X. Li, M. Caricato, A. Marenich, J. Bloino, B. G. Janesko, R. Gomperts, B. Mennucci, H. P. Hratchian, J. V. Ortiz, A. F. Izmaylov, J. L. Sonnenberg, D. Williams-Young, F. Ding, F. Lipparini, F. Egidi, J. Goings, B. Peng, A. Petrone, T. Henderson, D. Ranasinghe, V. G. Zakrzewski, J. Gao, N. Rega, G. Zheng, W. Liang, M. Hada, M. Ehara, K. Toyota, R. Fukuda, J. Hasegawa, M. Ishida, T. Nakajima, Y. Honda, O. Kitao, H. Nakai, T. Vreven, K. Throssell, J. A. Montgomery, Jr., J. E. Peralta, F. Ogliaro, M. Bearpark, J. J. Heyd, E. Brothers, K. N. Kudin, V. N. Staroverov, T. Keith, R. Kobayashi, J. Normand, K. Raghavachari, A. Rendell, J. C. Burant, S. S. Iyengar, J. Tomasi, M. Cossi, J. M. Millam, M. Klene, C. Adamo, R. Cammi, J. W. Ochterski, R. L. Martin, K. Morokuma, O. Farkas, J. B. Foresman, and D. J. Fox. Gaussian 09 revision A.02. Gaussian Inc. Wallingford CT, 2016.

[43] Rudolf Pfeiffer, Christian Kramberger, Herwig Peterlik, Hans Kuzmany, Bernhard Kräutler, Manuel Melle-Franco, and Francesco Zerbetto. Ft-raman characterization of the antipodal bis-adduct of C_{60} and anthracene. *physica status solidi (b)*, 246:2794–2797, 2009.

[44] R. Moret, P. Launois, P.-A. Persson, and B. Sundqvist. First x-ray diffraction analysis of pressure polymerized C_{60} single crystals. *Europhysics Letters*, 40:55, 1997.

[45] V. A. Davydov, L. S. Kashevarova, A. V. Rakhmanina, V. Agafonov, H. Allouchi, R. Ceolin, A. V. Dzyabchenko, V. M. Senyavin, and H. Szwarc. Tetragonal polymerized phase of C_{60}. *Phys. Rev. B*, 58:14786–14790, 1998.

[46] V. A. Davydov, L. S. Kashevarova, A. V. Rakhmanina, V. M. Senyavin, R. Céolin, H. Szwarc, H. Allouchi, and V. Agafonov. Spectroscopic study of pressure-polymerized phases of C_{60}. *Phys. Rev. B*, 61:11936–11945, 2000.

[47] R. Moret, P. Launois, T. Wågberg, and B. Sundqvist. High-pressure synthesis, structural and raman studies of a two-dimensional polymer crystal of C_{60}. *Eur. Phys. J. B*, 15:253–263, 2000.

[48] R. Moret, T. Wågberg, and B. Sundqvist. Influence of the pressure–temperature treatment on the polymerization of C_{60} single crystals at 2gpa–700k. *Carbon*, 43:709 – 716, 2005.

[49] B. Narymbetov, V. Agafonov, V. A. Davydov, L. S. Kashevarova, A. V. Rakhmanina, A. V. Dzyabchenko, V. I. Kulakov, and R. Céolin. The crystal structure of the 2d polymerized tetragonal phase of C_{60}. *Chemical Physics Letters*, 367:157 – 162, 2003.

[50] G. Oszlányi and L. Forró. Two-dimensional polymer of C_{60}. *Solid State Communications*, 93:265–267, 1995.

[51] A. V. Dzyabchenko, V. N. Agafonov, and V. A. Davydov. Molecular interaction and crystal packing in products of polymerization of Fullerene C_{60} under high pressures. *Crystallography Reports*, 44:13–17, 1999.

[52] A. V. Okotrub, V. V. Belavin, L. G. Bulusheva, V. A. Davydov, T. L. Makarova, and D. Tománek. Electronic structure and properties of rhombohedrally polymerized C_{60}. *The Journal of Chemical Physics*, 115:5637–5641, 2001.

[53] Y. Iwasa, T. Arima, L.J. Rothberg, R.M. Fleming, O. Zhou, K.B. Lyons, S.-W. Cheong, R.C. Haddon, A.F. Hebard, and G.A. Thomas. Pressure-induced cross-linking of C_{60}. *Synthetic Metals*, 70:1407 – 1408, 1995.

[54] V. D. Blank, S. G. Buga, N. R. Serebryanaya, G. A. Dubitsky, S. N. Sulyanov, M. Y. Popov, V. N. Denisov, A. N. Ivlev, and B. N. Mavrin. Phase transformations in solid C_{60} at high-pressure-high-temperature treatment and the structure of 3d polymerized fullerites. *Physics Letters A*, 220:149 – 157, 1996.

[55] L. Marques, J. L. Hodeau, M. Núñez−Regueiro, and M. Perroux. Pressure and temperature diagram of polymerized fullerite. *Phys. Rev. B*, 54:12633–12636, 1996.

[56] V. A. Davydov, V. Agafonov, A. V. Dzyabchenko, R. Céolin, and H. Szwarc. Packing models for high-pressure polymeric phases of C_{60}. *Journal of Solid State Chemistry*, 141:164 – 167, 1998.

[57] A. V. Dzyabchenko, V. N. Agafonov, and V. A. Davydov. Theoretical molecular packings and the structural model of solid-phase polymerization of fullerene C_{60} under high pressures. *Crystallography Reports*, 44:18–24, 1999.

[58] T. Miyake and S. Saito. Geometry and electronic structure of rhombohedral C_{60} polymer. *Chemical Physics Letters*, 380:589 – 594, 2003.

[59] J. Yang, J. S. Tse, and T. Iitaka. First-principles investigation on the geometry and electronic structure of the three-dimensional cuboidal C_{60} polymer. *The Journal of Chemical Physics*, 127:134906, 2007.

[60] G. Kresse, M. Marsman, and J. Furthmüller. Vasp the guide. 2016. url: https://cms.mpi.univie.ac.at/vasp/vasp/vasp.html, Retrieved August 25, 2017.

[61] S. Margadonna, D. Pontiroli, M. Belli, T. Shiroka, M. Riccò, and M. Brunelli. Li_4C_{60}: A polymeric fulleride with a two-dimensional architecture and mixed interfullerene bonding motifs. *Journal of the American Chemical Society*, 126:15032–15033, 2004.

[62] P. A. Heiney, J. E. Fischer, A. R. McGhie, W. J. Romanow, A. M. Denenstein, J. P. McCauley Jr., A. B. Smith, and D. E. Cox. Orientational ordering transition in solid C_{60}. *Phys. Rev. Lett.*, 66:2911–2914, 1991.

[63] W. I. F. David, R. M. Ibberson, J. C. Matthewman, K. Prassides, T. J. S. Dennis, J. P. Hare, H. W. Kroto, R. Taylor, and D. R. M. Walton. Crystal structure and bonding of ordered C_{60}. *Nature*, 353:147–149, 1991.

[64] J. R. D. Copley, W. I. F. David, and D. A. Neumann. Structure and dynamics of buckyballs. *Neutron News*, 4:20–28, 1993.

[65] C. G. Shull, W. A. Strauser, and E. O. Wollan. Neutron diffraction by paramagnetic and antiferromagnetic substances. *Phys. Rev.*, 83:333–345, 1951.

[66] A. Danielian. Ground state of an ising face-centered cubic lattice. *Phys. Rev. Lett.*, 6:670–671, 1961.

[67] A. Danielian. Low-temperature behavior of a face-centered cubic antiferromagnet. *Phys. Rev.*, 133:A1344–A1349, 1964.

[68] A. V. Talyzin, F. Langenhorst, N. Dubrovinskaia, S. Dub, and L. S. Dubrovinsky. Structural characterization of the hard fullerite phase obtained at 13 GPa and 830 K. *Phys. Rev. B*, 71:115424, 2005.

[69] C. Kittel. *Introduction to Solid State Physics*. John Wiley & Sons, Inc., New York, 6th edition, 1986.

[70] C. Hammond. *The Basics of Crystallography and Diffraction*. International Union of Crystallography texts on crystallography. OUP Oxford, 2009.

[71] H. T. Stokes and M. Rakitin. Poscar2cif. 2015. url: http://han.ess.sunysb.edu/poscar2cif/, Retrieved September 08, 2017.

Appendices

Known C_{60} Polymers Relaxed Fractional Coordinates

Table 1: Fractional atomic coordinates of 1D orthorhombic phase after ionic, cell shape and volume relaxation, structure space group $Immm$ and lattice parameters in Å.

atom	x	y	z
C(1)	0.22433	0.06610	0.00000
C(2)	-0.35133	-0.25491	0.42048
C(3)	0.00000	-0.32464	-0.07668
C(4)	-0.30481	-0.36513	0.37155
C(5)	-0.42461	-0.21660	0.34335
C(6)	-0.33382	-0.43135	0.24778
C(7)	-0.45256	-0.28462	0.21432
C(8)	-0.40693	-0.38882	0.16560
C(9)	0.05137	0.00000	-0.41257
lattice parameters	a(Å)	b(Å)	c(Å)
	9.11	10.57	15.60

Table 2: Fractional atomic coordinates of 2D tetragonal phase after ionic, cell shape and volume relaxation, structure space group $Immm$ and lattice parameters in Å.

atom	x	y	z
C(1)	-0.24753	-0.41981	0.34370
C(2)	-0.16502	-0.37021	0.41200
C(3)	-0.37202	-0.34234	0.31781
C(4)	-0.21529	-0.24839	0.45524
C(5)	-0.41939	-0.21343	0.36157
C(6)	-0.34066	-0.16633	0.42880
C(7)	0.08788	0.41185	0.00000
C(8)	0.00000	0.07710	-0.20907
C(9)	0.41292	0.00000	-0.04856
lattice parameters	a(Å)	b(Å)	c(Å)
	9.09	9.09	16.48

Table 3: Fractional atomic coordinates of 2D rhombohedral phase after ionic, cell shape and volume relaxation, structure space group $R\bar{3}m$ and lattice parameters in Å.

atom	x	y	z
C(1)	-0.46060	-0.09433	0.01055
C(2)	-0.39107	-0.11864	0.05923
C(3)	-0.18913	0.18913	0.06790
C(4)	-0.22578	0.22578	0.02183
C(5)	-0.01647	0.27356	0.08762
C(6)	-0.15595	-0.00179	0.11793
lattice parameters	a(Å)	b(Å)	c(Å)
	9.21	9.21	26.53

Table 4: Fractional atomic coordinates of 3D cuboidal phase after ionic, cell shape and volume relaxation, structure space group $Immm$ and lattice parameters in Å.

atom	x	y	z
C(1)	-0.30321	-0.16420	0.39897
C(2)	-0.40662	-0.10306	0.32711
C(3)	-0.44492	-0.21872	0.20061
C(4)	-0.28609	-0.33478	0.36540
C(5)	-0.21500	-0.09332	0.29438
C(6)	-0.39309	-0.35919	0.16694
C(7)	0.05188	0.00000	-0.34924
C(8)	0.22323	0.08223	0.00000
C(9)	0.00000	-0.36729	-0.07624
lattice parameters	a(Å)	b(Å)	c(Å)
	8.63	8.51	13.15